NASA TN D-1035

TECHNICAL NOTE
D-1035

TWO INSTRUMENTS FOR MEASURING DISTRIBUTIONS

OF LOW-ENERGY CHARGED PARTICLES IN SPACE

By Michel Bader, Thomas B. Fryer,
and Fred C. Witteborn

Ames Research Center
Moffett Field, Calif.

NATIONAL AERONAUTICS AND SPACE ADMINISTRATION

WASHINGTON

July 1961

NATIONAL AERONAUTICS AND SPACE ADMINISTRATION

TECHNICAL NOTE D-1035

TWO INSTRUMENTS FOR MEASURING DISTRIBUTIONS OF LOW-ENERGY CHARGED PARTICLES IN SPACE

By Michel Bader, Thomas B. Fryer,
and Fred C. Witteborn

SUMMARY

Current estimates indicate that the bulk of interplanetary gas consists of protons with energies between 0 and 20 kev and concentrations of 1 to 10^5 particles per cm^3. Methods and instrumentation for measuring the energy and density distribution of such a gas are considered from the standpoint of suitability for space vehicle payloads. It is concluded that electrostatic analysis of the energy distribution can provide sufficient information in initial experiments. Both magnetic and electrostatic analyzers should eventually be used.

Several instruments designed and constructed at the Ames Research Center for space plasma measurements, and the methods of calibration and data reduction are described. In particular, the instrument designed for operation on solar cell power has the following characteristics: weight, 1.1 pounds; size, 2 by 3 by 4 inches; and power consumption, 145 mw. The instrument is designed to yield information on the concentration, energy distribution, and the anisotropy of ion trajectories in the 0.2 to 20 kev range.

INTRODUCTION

The state of knowledge about the composition and energy distribution of matter in interstellar space has, until recently, depended to a large extent on interpretation of indirect evidence, and on the construction of plausible theoretical models whose predictions were in general agreement with this evidence. By means of such techniques it has been deduced that the interstellar gas probably consists of a thermal background of protons and electrons, with a small percentage of neutral hydrogen atoms, and smaller traces of other substances. It is further indicated that there exist in the solar system relatively high-density low-energy streams of protons, sometimes called solar winds, which are generally associated with solar activity. Information on cosmic rays, the higher energy particles, has been obtained more directly, since many of these particles can penetrate the earth's magnetic field and reach the earth's atmosphere. Order-of-magnitude estimates for the particle populations involved are as follows:

	Concentration, particles cm^{-3}	Particle flux, particles $cm^{-2}sec^{-1}$	Energy flux, gev $cm^{-2}sec^{-1}$	References
Interstellar neutral gas	1	---	---	1,2,3
Interstellar proton gas (ev)	10^2	---	---	2,4,5,6
Solar wind, near earth (kev)	10^2 to 10^5	10^9 to 10^{13}	10^3 to 10^8	7-12
Earth's radiation belts (Mev)	10^{-5}	10^3 to 10^5	10^3 to 10^5	13
Cosmic rays, near earth (gev)	10^{-10}	1	1	11,12

While these numbers are admittedly crude, they do point out the importance of the low-energy component of the interstellar medium: this portion contains higher numbers of particles and produces higher energy fluxes by several orders of magnitude than all other known components. Their low penetrating power has made them impossible to be observed directly from the earth, and they are not a biological hazard to space travelers. On the other hand, they are of prime importance in questions such as those of the origin and distribution of matter in space, the energy balance in the upper atmosphere of the earth, and possible surface damage to space vehicles - to name but a few of the problems.

With the advent of space flight, it has become possible to perform experiments yielding direct information on the interplanetary medium of the solar system. The first such experiments have dealt with the high-energy particles, which were known to exist and for which the art of detection had been advanced by nuclear and cosmic-ray physicists. These experiments have increased our information on cosmic rays, and they have led to the discovery by Van Allen and co-workers of the trapped radiation layers about the earth. It is in principle possible to obtain very detailed information on the important low-energy particles by means of appropriate combinations of existing techniques. Specifically, energy analysis can be obtained electrostatically, and mass analysis, magnetically. The electric and magnetic fields can be swept to cover the expected energy and momentum ranges.

In view of the above considerations, a program was started with objective the eventual detailed mapping and understanding of low-energy particle distributions in accessible regions of space. In the following sections we shall discuss the design principles and feasibility of electromagnetic analysis, and the specific design, construction and calibration of two electrostatic analyzers developed at the Ames Research Center of the NASA for space-vehicle payloads.

PRINCIPAL SYMBOLS

$A_1, A_2, B_1, B_2,$	curve-fitting parameters (eq. (23))
b	half the length of the entrance slit
c	half the width of the entrance slit
DTU	digital telemetry unit
E	particle kinetic energy
E_a	nominal acceptance energy for a given plate voltage V_a
ΔE	theoretical range of particle energies accepted by analyzer at any given angle and plate voltage
e	electric charge on a particle
f	acceptance function (For a monoenergetic, unidirectional beam of particles, f is the ratio of collector current to current incident on the entrance slit.)
I	current
I_{CBO}	transistor leakage current
I_c	collector current
I_e	ion current into entrance slit
k	Boltzmann constant
m	particle mass
N	total particle concentration
n	differential particle concentration or distribution function
r	radial distance from center of curvature of analyzer plates
r_0, r_1, r_2	mean, inner, and outer values of r, respectively, for gap between analyzer plates
Δr	plate separation, $r_2 - r_1$
S	area of entrance slit

T	absolute temperature
t	slit dimension, either length or width
u	velocity of particle, undisturbed by plasma sheath around vehicle
V_a	voltage difference between outer and inner analyzer plates
V_s	voltage drop across plasma sheath between undisturbed space and vehicle
v	velocity of particle as it enters analyzer entrance slit
w	component of v normal to entrance slit
x,y,z	rectangular Cartesian coordinates, centered on entrance slit (see sketch (d))
α	angle of incidence in plane normal to entrance slit (see sketch (d))
α_1, α_2	values of α outside vehicle plasma sheath and at entrance slit, respectively (see sketch (e))
β	transistor current gain for a common emitter configuration
δ	$\frac{\Delta r}{2r_o}$
ϵ	$\frac{E}{\epsilon_N}$
ϵ_a	$\frac{E_a}{\epsilon_N}$
ϵ_m	curve-fitting parameter (eq. (23))
ϵ_N	normalizing energy chosen for convenience; for example, $\epsilon_N = kT$ for a Maxwellian distribution
η	curve-fitting parameter (eq. (23))
θ	polar angle of incidence (see sketch (d))
ν	parameter in trial angular distribution function (see eqs. (24a,b,c))
ξ	$\frac{\Delta r}{r_1}$

ρ, ρ_1, ρ_2	$\frac{r}{r_o}, \frac{r_1}{r_o}, \frac{r_2}{r_o}$
σ	curve-fitting parameter (eq. (23))
Φ_1	flux of ions on entrance slit
Φ_2	flux of ions on collector, corrected for secondary electron emission; hence $e\Phi_2 = I_c$
φ	azimuthal angle of incidence (see sketch (d))

GENERAL DESIGN CONSIDERATIONS

There are two important features to be considered in the experiments, in addition to size, weight, and power consumption limitations. First, the particles of interest have a relatively large range of energies and momenta; and second, they are likely to reach the vehicle from directions distributed over a large solid angle.

In a conventional mass spectrometer, ions are created at essentially thermal energies in a "source." They are then extracted by a system of slits which collimate them into a well-defined beam and accelerate them electrostatically to a well-defined energy (large compared to thermal). The beam enters a magnetic field, in which particles of different momenta follow paths of different curvature and are hence separated. To detect a range of particle masses, one then has a choice of varying the accelerating electric fields, varying the magnetic field, or using a series of collectors, one for each of the momenta separated by the magnet. The size and power consumption limitations imposed on space vehicle payloads preclude all but the electric field variation. Since, in addition, the "source" in space is not of negligibly small energy, a well-defined beam, energywise, cannot be obtained by electrostatic acceleration alone.

The problem of mass and energy determination is first simplified by requiring that the instrument detect only one mass (say, protons or alpha particles) as a function of energy. Then, by a floating electrode arrangement, as shown schematically in figure 1, the proper mass current as a function of energy can be obtained with a fixed collector and a permanent magnet. The particle beam is admitted through a slit in the vehicle surface, then accelerated by a variable voltage to a second aperture. It then enters a fixed-voltage, curved-plate, electrostatic analyzer whose mean potential is that of the second aperture. Only the particles with a given energy can get through, the energy being determined by the voltage across the analyzer plates. These particles then enter the fixed field of a permanent magnet, so that only those with a predetermined momentum can get through. For a given fixed energy and

momentum only particles of a predetermined mass can reach the collector, and their initial energy is the difference between the analyzer acceptance energy and the (variable) accelerating voltage. Note that the magnet must be at the second aperture potential. Design calculations have been made for such an instrument with the following results. For the detection of protons in the energy range 0-20 kev, the mean electrostatic radius of curvature would be 1 inch; the plate voltage difference, 1.6 kv; the variable supply, ±10 kv; and the magnetic field, 5,000 gauss. The total weight of the device would be about 3 pounds.

It is possible to simplify the above instrument as follows. Since flux is concentration times velocity, the particle current at a given energy is inversely proportional to the square root of the particle mass. Hence it would be a good approximation to correct the data assuming that the particles are 85 percent protons and 14 percent alphas, as estimated for cosmic rays, and forego mass analysis. This procedure is especially attractive to use for the first few experiments in which the maximum probable error so introduced, about 5 percent, is unimportant when one considers other uncertainties in the experiment and the saving in weight (no magnet needed). If, then, we dispense with the magnet, the energy of the beam at the electrostatic analyzer exit need no longer be fixed. Hence, we can leave out the second aperture, and change the energy accepted by varying the analyzer plate voltages. This should be done in such a way as to keep the mean potential zero, that is, by driving the inner and outer plates by equal voltages of opposite sign. This would eliminate large entrance and exit fields, and minimize the voltage to ground, easing insulation problems. We thus arrive at the greatly simplified arrangement shown in figure 2. Such instruments have been built and tested, and we turn now to a detailed discussion of their design.

ENERGY ANALYZER CHARACTERISTICS

Two easily machinable shapes for electrostatic analyzer plates are cylinders and spheres. For most laboratory applications, the geometric cross section of the beam is small and the incident direction is well defined. Under these conditions the curvature in the plane perpendicular to the beam path is insignificant. The only important resulting difference is that the focal points of a spherical analyzer are 180° apart, while those of a cylindrical analyzer are 127° apart, so that a cylindrical analyzer can be made somewhat smaller. Comparable resolutions can be obtained with the two shapes. Since, in addition, cylindrical plates are somewhat easier to machine, cylindrical analyzers are the ones in general usage.

For good energy resolution an analyzer must have a plate separation small compared to the radius of curvature. Since a small instrument is desirable, a narrow entrance slit is required, but a large entrance slit

area is needed to collect a detectable particle current. Hence we are led to a long, narrow slit, and must consider in more detail the differences in behavior between spherical and cylindrical electrostatic fields, in particular for large angles of incidence.

The incidence angles of the ion at the aperture, α and φ, are defined in sketches (a) and (b) for the two geometries. The dependence

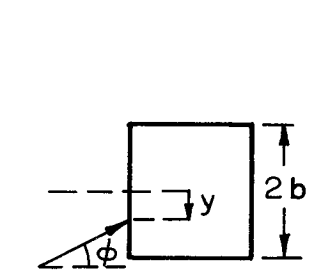

Sketch (a)

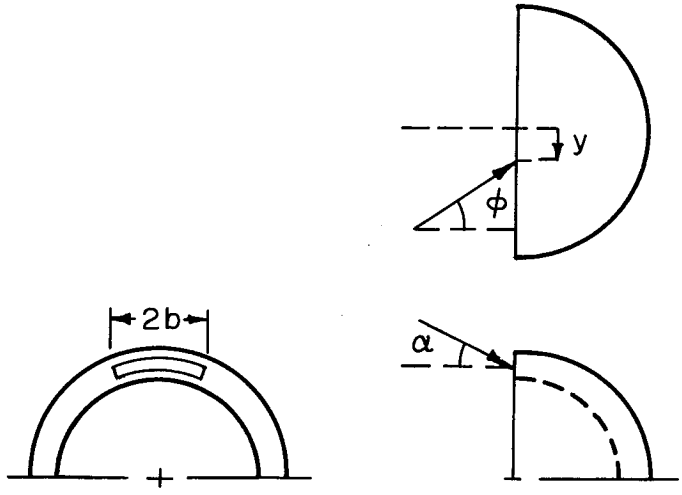

Sketch (b)

of energy acceptance on α is essentially the same for cylindrical and spherical plates. The dependence on φ, however, has some important characteristics which are different in the two cases. Consider the incident velocity u to be in the plane $\alpha = 0$, and let the plate voltage difference V_a be set to accept a certain energy E_a, corresponding to a velocity w for protons. In the cylindrical case, only the component $u \cos \varphi$ is affected by the field, so that a large range of velocities is accepted at one setting, namely those satisfying $w = u \cos \varphi$. The only limitation is that $u \sin \varphi$ must not be so large that the particle goes out the sides before being collected (sketch (a)). This limitation is a function of y, $2b$, u, and φ which can be modified by placing collimating slits ahead of the entrance slit, and by making $2b$, the slit length, less than the total plate width. In the spherical case, the particle follows a great circle arc regardless of the angle φ (sketch (b)). Hence the spherical analyzer accepts all particles of energy E_a, regardless of their incidence angle φ.

If, then, we wish to detect a random distribution of particles, we can get more current at a given energy setting by using a spherical analyzer. If we wish to detect a directed particle beam, the cylindrical analyzer (with b small compared to the plate radius) gives the direction of motion as well as the energy of the particles provided the vehicle is oriented so that the analyzer accepts the beam. The spherical analyzer requires only that the vehicle be oriented normally to the wind in one plane; this increases the chances of detection, but leaves a directional

ambiguity. The orientations can be varied periodically through the natural spin motion of the vehicle or by providing a rotating platform on a nonspinning vehicle. Other possibilities, involving more than one instrument on a vehicle, can easily be imagined.

The single energy E_a considered above really consists of a small range of energies ΔE near E_a. This range and the voltage V_a corresponding to E_a can be estimated as follows: Let the beam be assumed to enter halfway between the plates, and consider an entrance point y and an angle φ (sketch (a) or (b)) for which edge effects are negligible. Let the inner and outer analyzer plate radii be r_1 and r_2; $r_o = (r_1 + r_2)/2$; and r, γ be the radial and angular coordinates of the beam path as measured, respectively, from the center of plate curvature and from the plane of the entrance slit (see sketch (c)). Let V_a denote the voltage difference between the plates. Then for $\alpha = 0$ we obtain the condition for an equilibrium orbit r by equating the electrical and inertial (centrifugal) forces on a beam particle:

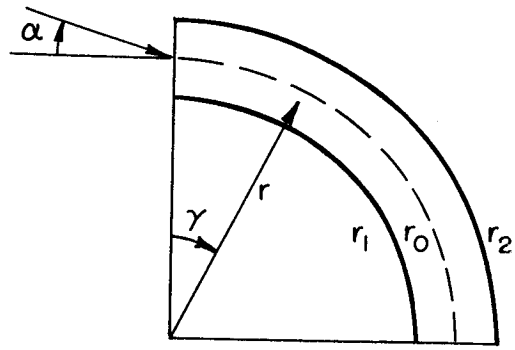

Sketch (c)

$$\frac{1}{\ln(r_2/r_1)} \frac{eV_a}{r} = \frac{mv^2}{r} = \frac{2E}{r} \qquad \text{(cylindrical case)} \qquad (1)$$

$$\frac{r_1 r_2}{r_2 - r_1} \frac{eV_a}{r^2} = \frac{mv^2}{r} = \frac{2E}{r} \qquad \text{(spherical case)} \qquad (2)$$

These reduce to the following equations for $E = E_a$ and $r = r_o$:

$$\frac{E_a}{eV_a} = \frac{1}{2} \frac{1}{\ln(r_2/r_1)} = \frac{1}{2} \frac{1}{\ln(1 + \xi)} = \frac{1}{2\xi} \left(1 + \frac{\xi}{2} - \frac{\xi^2}{12} + \cdots\right) \qquad (3)$$

for the cylindrical case, while in the spherical case we have

$$\frac{E_a}{eV_a} = \frac{1}{2} \frac{r_1 r_2}{r_2 - r_1} \frac{1}{r_o} = \frac{1}{2\xi} \frac{1 + \xi}{1 + \xi/2} = \frac{1}{2\xi} \left(1 + \frac{\xi}{2} - \frac{\xi^2}{4} + \cdots\right) \qquad (4)$$

where $\xi = (r_2 - r_1)/r_1 = \Delta r/r_1$. Note that, for small ξ, the analyzer constant E_a/eV_a is the same for spherical and for cylindrical analyzers.

To calculate the energy resolution, we need to know the path of a particle entering with energy E at angle α when V_a is set for E_a. That the paths are different in the spherical and cylindrical cases can be realized immediately from the fact that the focal lengths are different for paraxial rays (180° for the spherical geometry and 127° for the cylindrical). It is suggested by the above equations that the differences are small and that the characteristic behaviors are similar. We shall avoid the difficulties of solving the equations of motion for a logarithmic potential and consider the spherical case in which the $1/r$ dependence of the potential leads to the familiar Kepler orbit

$$r = \frac{l^2/k}{1 + \bar{\epsilon}\cos(\gamma - \gamma')} \tag{5}$$

where l is the particle angular momentum, $\bar{\epsilon}$ is the eccentricity, and k, in this case, is $eV_a r_1 r_2/(r_2 - r_1)$. The constants l and γ' are fixed by the entrance conditions ($\gamma = 0$).

We then compute from equation (5) the maximum and minimum values of $\rho = r/r_o$ as functions of E and α, and require that

$$\rho_1 = \frac{r_o - \Delta r/2}{r_o} = 1 - \delta \leq \rho \leq 1 + \delta = \frac{r_o + \Delta r/2}{r_o} = \rho_2 \tag{6}$$

There result finally the following conditions on E and α:

$$\tan^2\alpha \leq \delta^2 \tag{7}$$

$$\frac{2\rho_1\delta(1 + \tan^2\alpha)}{1 - \rho_1^2(1 + \tan^2\alpha)} \leq \frac{E}{E_a} \leq \frac{2\rho_2\delta(1 + \tan^2\alpha)}{(1 + \tan^2\alpha)\rho_2^2 - 1} \tag{8}$$

where ρ_1, ρ_2, and δ are defined by equation (6), and E_a is the energy for which the analyzer is set, in accordance with equation (4). For good resolution, δ should be small compared to unity, in which case equations (7) and (8) can be written

$$\alpha^2 \leq \delta^2 \tag{9}$$

$$1 - \frac{\delta}{2}\left\{1 - \left(\frac{\alpha}{\delta}\right)^2 + \frac{\delta}{2}\left[1 - \left(\frac{\alpha}{\delta}\right)^4\right] + \cdots\right\}$$

$$\leq \frac{E}{E_a} \leq 1 + \frac{\delta}{2}\left\{1 - \left(\frac{\alpha}{\delta}\right)^2 - \frac{\delta}{2}\left[1 - \left(\frac{\alpha}{\delta}\right)^4\right] + \cdots\right\} \tag{10}$$

We see that the maximum range ΔE of accepted energies occurs for $\alpha = 0$, in which case $\Delta E/E_a \approx \delta$.

ESTIMATES OF COLLECTOR CURRENTS

The analyzer constants and the resolution (eqs. (3), (4), and (10)) are, in practice, obtained experimentally. This is true also of the ratio of collector current to flux on the entrance slit (fig. 2). It is, however, necessary to develop analytical expressions relating these quantities to the possible particle distributions in space in order to obtain design estimates of collector currents, and later to reduce the data.

Let us choose a rectangular Cartesian coordinate system, as depicted in sketch (d), in which the slit is in the y-z plane, centered at the

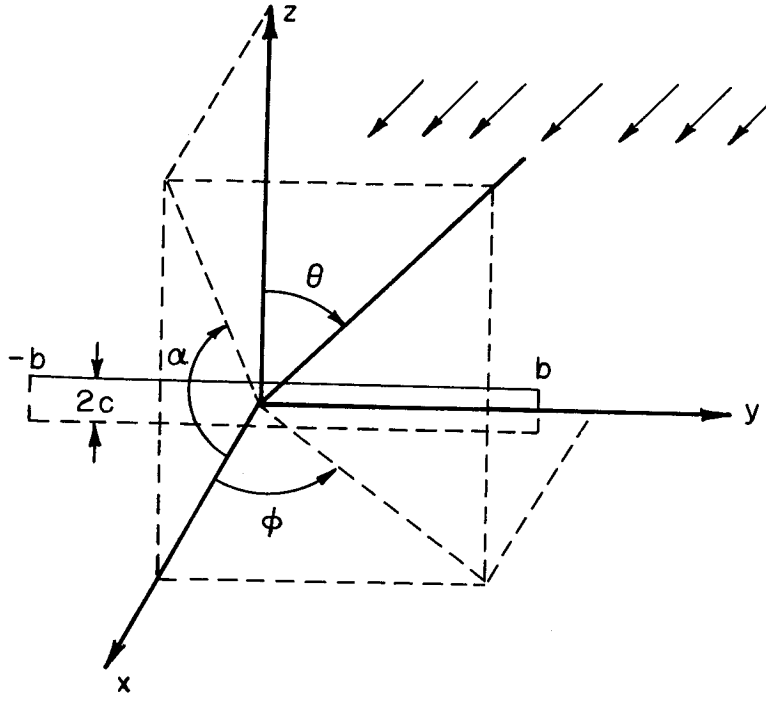

Sketch (d)

origin, and with its long dimension along the y axis. We then introduce the angular coordinates of the beam velocity vector, the polar angle θ measured from the z axis, and the azimuthal angle φ measured from the x axis. A useful angle will turn out to be α, the angle between the x axis and the projection of the particle direction on the x-z plane. The relationship between α, θ, and φ is:

$$\tan \alpha \tan \theta \cos \varphi = 1 \tag{11}$$

The flux of particles with speeds in the interval u to $u + du$, in the direction range θ to $\theta + d\theta$ and φ to $\varphi + d\varphi$, onto an element of slit area $dy\ dz$ at y, z, will then be

$$d\Phi_1 = n(u, \theta, \varphi) u \sin^2\theta \cos \varphi \, d\theta \, d\varphi \, dy \, dz \, du \tag{12}$$

where $n(u, \theta, \varphi)$ is the number of particles per unit volume and unit solid angle with speed u in the direction θ, φ.

A 4 0 3

Only a fraction of the incident flux will be measured, namely, that which is accepted by the analyzer. This fraction will, in general, be a function f of y, z, θ, φ and $E = mu^2/2$. Let the dimension c be small enough that no physical quantities vary appreciably over $-c \leq z \leq c$, and express u in terms of $\epsilon = E/\epsilon_N$, where ϵ_N is any convenient energy parameter. The differential collector flux from a length of slit dy is then:

$$d\Phi_2 = 2c \left(\frac{2\epsilon_N}{m}\right)^{1/2} n(\epsilon, \theta, \varphi) f(y, \theta, \varphi, \epsilon) \epsilon^{1/2} \sin^2\theta \cos \varphi \, d\theta \, d\varphi \, dy \, d\epsilon \tag{13}$$

For design purposes, consider first a high-energy-directed particle beam normally incident on the analyzer entrance slit. When the analyzer plates reach the proper voltage, essentially all the flux on the slit is collected, and the resulting flux is

$$\Phi_1 = \Phi_2 = NuS \tag{14}$$

where N is the number of particles per unit volume and S is the slit area. For a proton wind incident on a 1 cm^2 slit, the following probable extremes in current exist: For $u = 500$ km/sec and $N = 10^2$ protons/cm^3, $e\Phi_2 = I = 8\times10^{-10}$ amp; for $u = 2000$ km/sec and $N = 10^5$ protons/cm^3, $I = 3\times10^{-6}$ amp. These values are well within the detecting capabilities of electrometer circuits, so that they satisfy the requirement of continuously measurable current.

As another example, consider a thermal, Maxwellian particle distribution and neglect such distortions as may be introduced by local electric or magnetic fields. Then, with $\epsilon_N = kT$,

$$n(\epsilon, \theta, \varphi) = \frac{N}{2}\left(\frac{1}{\pi}\right)^{3/2} \epsilon^{1/2} e^{-\epsilon} \tag{15}$$

In the spherical case, let f be independent of y. From equation (10) it is seen that $\Delta E/E_a \approx \delta[1 - (\alpha/\delta)^2]$, and equation (11), for small α, reduces to

$$\theta = \frac{\pi}{2} - \alpha \cos \varphi \tag{16}$$

Assume that f is unity over the acceptance range and zero outside. Then the collector flux will be, approximately,

$$\Phi_2 = \frac{NS}{\pi}\left(\frac{kT}{2\pi m}\right)^{1/2} \epsilon_a \epsilon e^{-\epsilon} \int_{-\frac{\pi}{2}}^{\frac{\pi}{2}} \int_{\frac{\pi}{2} - \delta\cos\varphi}^{\frac{\pi}{2} + \delta\cos\varphi} \delta \left[1 - \left(\frac{\alpha}{\delta}\right)^2\right] \cos\varphi \, d\theta \, d\varphi \tag{17}$$

where $\epsilon_a = E_a/kT$, ϵ is assumed constant over the range of integration, and $\sin^2\theta \approx 1 - \alpha^2\cos^2\varphi$ has been set equal to unity. The integration of equation (17) with α given by equation (16) yields

$$\Phi_2 = NS\left(\frac{kT}{2\pi m}\right)^{1/2} \delta^2 \epsilon_a \epsilon e^{-\epsilon} \tag{18}$$

The maximum flux occurs at $\epsilon = 1$, and this must also be the value of ϵ_a in the absence of distorting fields. Assuming a 1 cm^2 slit and a resolution parameter $\delta = 0.1$, we find the following possible extremes in current: For $N = 10^2$ protons/cm^3 and $T = 10^3$ °K, $e\Phi_2 = I \approx 10^{-14}$ amp; for $N = 10^4$ protons/cm^3 and $T = 10^6$ °K, $I \approx 10^{-11}$ amp.

A 4 0 3

ELECTRON DISTRIBUTIONS AND VEHICLE POTENTIAL

A vehicle traveling through the space plasma may acquire an electrostatic potential different from that of the medium. This potential may be of sufficient magnitude to affect the energies and trajectories of charged particles in the vicinity of the vehicle, and hence introduce an error in the determination of these quantities. There are several phenomena which can give rise to the accumulation of charge on a space vehicle. The most significant ones appear to be photoelectron emission, secondary electron emission due to ion or electron bombardment, and effects due to differences between positively and negatively charged particle fluxes on the vehicle.

Secondary and photoelectrons are normally returned to the emitting surfaces by potentials of less than 300 volts. Hence electron ejection can give rise to maximum positive vehicle potentials of this magnitude. In a neutral plasma in thermal equilibrium, the vehicle potential would tend to be negative because of higher electron than ion flux (refs. 14 and 15). The negative potential from this effect could be of the order of 300 volts in a 10^5 °K plasma. Possible flux difference effects in radiation belts or in the path of solar winds cannot be estimated

accurately because of insufficient data. It is not known, for example, whether proton winds are accompanied by electrons of the same velocity or the same energy, or by some other electron distribution (ref. 16). Resulting vehicle potentials could be in the kilovolt range for certain distributions.

In the case of a positively charged vehicle, an electron sheath forms around the vehicle; similarly, a negatively charged vehicle gives rise to a positive ion sheath. The effects on particle detection of potential gradients near the vehicle can be visualized as follows: Let the particles be incident on a virtual, or effective, analyzer entrance slit as seen by the undisturbed plasma outside the sheath. As a simple first approximation, assume that on the vehicle side of the virtual slit all particles are subjected to a normal, uniform potential gradient. Let the real slit be rectangular, and let a particle enter the sheath in a plane including one of the slit dimensions t (see sketch (e)) and at

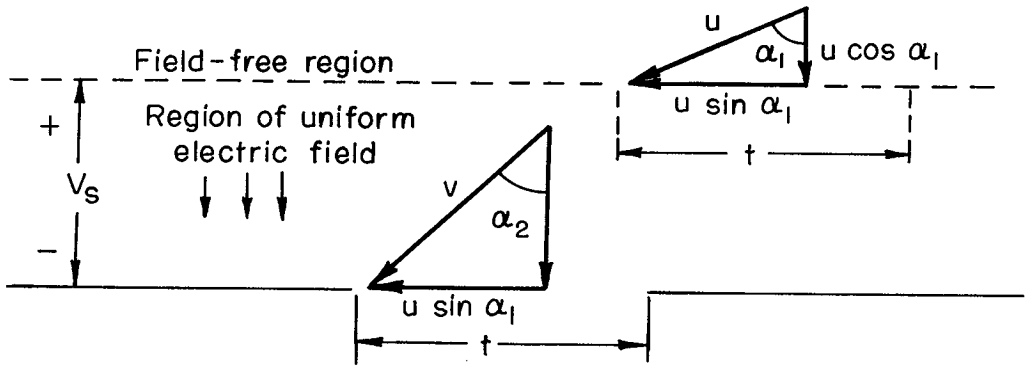

Sketch (e)

an angle α_1 to the normal to the slit plane. The particle reaches the slit plane with a velocity v given by

$$v^2 = \frac{2eV_s}{m} + u^2 \tag{19}$$

where e and m are the charge and mass of the particle and V_s is the sheath potential drop. The angle from the normal at the real slit, α_2, is given by

$$\sin \alpha_2 = \frac{u}{v} \sin \alpha_1$$

Note that the virtual slit is displaced from the real slit along the direction of t, but that the dimensions of the two slits are the same. The displacement is small if $u \sin \alpha_1 << v \cos \alpha_2$, which is a condition that the resolution of the analyzer imposes. Hence one effect of the sheath is simply to alter the angular range from which particles of a given speed are collected. This range is increased if e and V_s have

the same sign; otherwise it is decreased. A more serious effect is that all particles with incident energies small compared to the potential drop either reach the real slit with essentially the same energy, or do not reach it at all, depending on the sign of their charge.

Consider now some representative velocities and corresponding energies:

	Vehicle velocity, 10 km/sec	Slow solar wind, 500 km/sec	Fast solar wind, 2,000 km/sec
Electrons	2.8×10^{-4} ev	0.7 ev	11 ev
Protons	0.5 ev	1.3 kev	21 kev

It is apparent that electron analysis (with reversed plate voltages on the electrostatic analyzer) would be difficult in the range of interest. In a solar wind, their maximum energy would be some 10 ev directed, with a possible 100 ev thermal. In the outer atmosphere, thermal electrons can be expected in the 0 to 10 ev range. It is important, then, that vehicle potential measurements be performed. If these potentials are indeed in excess of 100 volts, the analysis of the distribution of low-energy electrons will be complicated by the need for compensating fields. Since there seems to be little evidence for appreciable electron fluxes in the kev range, it is preferable to utilize the limited allotted payload space for positive ion analysis. It must be pointed out that positive ion analysis in the thermal range is subject to the same difficulties as is electron analysis. It is the evidence for solar winds and medium energy auroral protons which makes the experiment attractive.

FIRST INSTRUMENT

Design and Characteristics

The energy analyzer was originally planned for solar wind measurements on a deep space probe. Payload space was, however, first allocated on a sounding-rocket probe, the Scout No. 2, which was to reach an altitude of only 16,000 km. The flight time was to be about three hours and the maximum velocity about 6 km/sec. Since the time available for building the analyzer was limited by the launching schedule, some compromises had to be made in its design. The resulting instrument is a modification of the solar wind detector rather than a completely redesigned analyzer optimized for low altitude studies.

Because of interference from heavier ions, clearly interpretable data in terms of protons can be expected only above 2,000 km (without magnetic analysis). Below this altitude, data reduction should be based on relative density estimates, such as those of Johnson (ref. 5). In the 2,000 to 8,000 km range, one expects a thermal distribution of protons with energies of the order of 1 ev and concentrations of 10^3 to 10^4

particles/cm^3. The corresponding collector current, for a 1 cm^2 slit, is 10^{-14} amp. This figure together with the uncertainty in vehicle potential made the contemplated altitude range the most difficult to design for: order-of-magnitude larger currents can only be obtained by correspondingly increasing the instrument size, which is clearly undesirable, or by decreasing the resolution, in which case the structure of the distribution is obscured. An additional difficulty is due to the vehicle velocity in conjunction with its trajectory: Since increased current sensitivity generally entails longer response times, altitude resolution must be compromised.

The instrument as designed on the basis of the above considerations is shown in figures 3 and 4. Cylindrical plates were chosen because they are easier to machine, and they give directional information which can be correlated with the data from aspect sensors in the payload. The physical dimensions give an energy acceptance $\Delta E/E \approx 0.1$ (see eq. (10)) and allow a 1 cm^2 slit. The useful sensitivity range is 5×10^{-14} to 10^{-10} amp. The analyzer plates are swept linearly and simultaneously from 0 to plus and minus 100 volts, respectively, in 10 seconds. The particle energy range covered is 0 to 2.5 kev, a compromise between higher resolution at the lower end and the chance of detecting kev-range particles along the anticipated trajectory. The package weighs 3 pounds, including the battery pack for a one-week lifetime. This lifetime means that a delay of a few days on the launching pad, after payload access is cut off, would not jeopardize the functioning of the instrument.

Electronics

The circuitry associated with space instrumentation is affected by the vehicle characteristics (e.g., spin rate) and the other on-board electronics (particularly power sources and telemetry systems). The purpose of the following discussion, and that in the next section, is to describe some solutions to the general circuitry problems and to show the versatility of the resulting systems by explaining in detail the way in which the basic techniques have been applied to meet the requirements of two specific payloads.

The circuit diagram of the instrument designed for use in the Scout No. 2 is shown in figure 5. The instrument has two primary functions to perform; namely, to measure low level currents in the 10^{-14} to 10^{-10} amp range, and to provide a sweep voltage for the analyzer plates. These two functions are almost completely independent and will be discussed in turn. The instrument requirements for the Scout No. 2 payload made simplifications possible, but an important consideration in determining the circuits was to provide a flexible system that could be easily modified for new applications. The electrometer current range, the analyzer plate voltage and sweep time, and the primary power sources

are some of the characteristics that may need to be varied on different vehicles. One other important design criterion is low power consumption consistent with long term reliability.

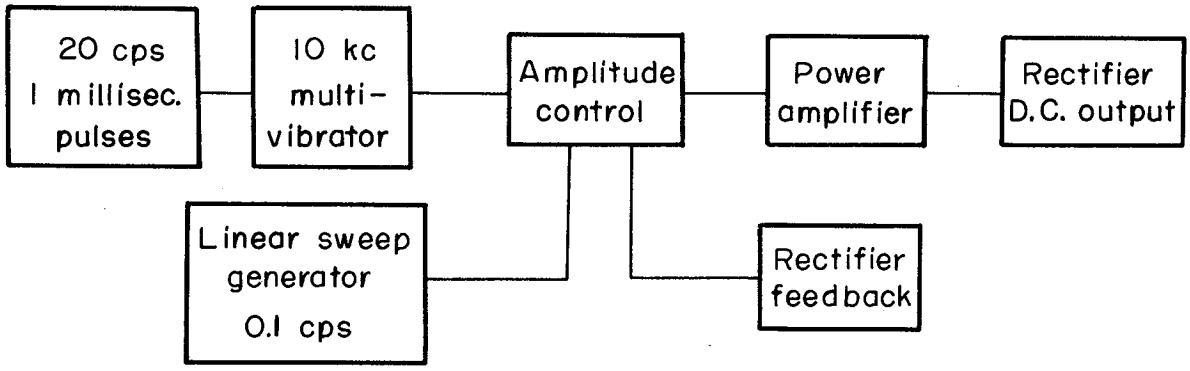

Sketch (f)

A block diagram of the high voltage sweep generator is shown in sketch (f). The system was originally designed for use at ±2500 v, but for a low altitude flight a plate voltage of ±100 v was desired. The use of an inverter transformer in the original design made possible a change in the turn ratio and a consequent change of sweep voltage without any circuit redesign. The high-voltage power supply is conservatively designed for load currents of 0 to 1 μa (the best estimate indicated that a 0.1 μa positive ion current might be expected under the most adverse conditions). The required output power at ±2500 v is therefore only 5 mw. To meet the requirement of minimum power consumption, it was necessary to design an inverter that would give good efficiency at these very low power levels.

The necessity of keeping the transformer small and light in weight is not compatible with the requirement of good efficiency so that a compromise had to be reached. A 1/4- by 1/4-inch hypersil core with a 1/4- by 1-inch window was selected as the largest size and weight that would be compatible with the rest of the instrument. Considerations of flux density, inductance, distributed capacity, and core loss versus frequency resulted in the selection of a 4000 turn secondary winding for ±2500 v dc maximum output, while operating at the 8 kc resonant frequency of this winding. The use of a voltage doubler increased the efficiency somewhat; but the 300 to 500 mw no-load power loss introduced primarily by the transformer was still greatly in excess of that required for good efficiency. Some means of reducing the core loss without increasing size was essential, then, if a highly efficient instrument was to evolve. Since no losses occur in the transformer when it is turned off, it was decided to pulse the system on for short periods only. The duration of the on and off periods (duty cycle) can be adjusted easily by changing capacitors in the miltivibrator to fit the load requirements. The pulse used in the instrument is a 1 msec burst at 8 kc followed by an off

period of 20 msec. This 20 to 1 duty cycle cuts the power requirement to less than 25 mw. Since the voltage is swept from a high voltage to zero, the average power required is approximately 12 mw.

In order to obtain a 0 to ±100 v sweep, the number of secondary turns was reduced to 300, and a 2200 μμf capacitor was added to keep the resonant frequency at 8 kc. Filter capacitors of 0.04 μf with a bleeder resistor of 22 meg give adequate filtering (2 volts ripple) at the 20 msec pulse rate used.

A 90-turn feedback winding is used on the transformer to regulate the high voltage output. The low voltage on this winding is rectified by the same means as the high voltage output to maintain a constant ratio between the feedback voltage and the output. A voltage doubler makes the plus and minus voltages equal to within 1 percent, even though the ac voltage does not have a symmetrical waveform. The transformer coupling is sufficiently tight that load changes are reflected at the feedback winding and regulated by the feedback amplifier.

A
4
0
3

Transistor T15 regulates the output by modulating the magnitude of the 8-kc inverter drive. The gain of the modulation and output amplifier (T13, T14, and T15) is such that only 1 μa or less is required to change the output from maximum voltage to zero. The input sweep voltage, 0 - 3 v, and the feedback rectified voltage, 0 - 30 v, are mixed with summing resistors at the base of T15. The loop gain of T13, T14, and T15 and the feedback winding is sufficient to give 1-percent regulation for 0 to 3 μa output loading, which gives a wide safety factor over the design figure of 1 μa.

An 8 kc symmetrical square wave for the HV inverter is obtained from a conventional multivibrator (T10, T11). Transistors T7, T8, and T9 form a nonsymmetrical multivibrator which generates 1 msec pulses spaced 20 msec apart. These pulses modulate the 8 kc multivibrator so that the 8 kc oscillations are on for only 1 msec.

A 0 to 3 v saw-tooth waveform with a 10-second period is generated by T16, T17, T18, and T19. When the voltage across the 100 μf capacitor reaches +3 v, the base-to-emitter voltage drop across T17 and T19, T19 starts conducting. Feedback through T17 and T18 results in regeneration and saturation of T19. When T19 is saturated, the relay is actuated, causing the 100 μf capacitor to be discharged. Transistor T19 remains saturated (and relay actuated) until the 15 μf capacitor discharges and regeneration causes T19 to open-circuit and the 100 μf capacitor to start recharging. The 15 μf capacitor gives approximately 1 second of relay operation and the 100 μf provides a 10-second sweep period.

A Victoreen No. 5800 electrometer tube was selected for the electrometer circuit because of its low filament power consumption (12 mw) and because of its low leakage current (10^{-13} to 10^{-15} amp). This tube has a very low mu, however, and limits operating gain to approximately

one-half. A balanced input (for good temperature compensation) transistor direct-coupled amplifier is used in a feedback circuit to the cathode of the tube to obtain an over-all input-output gain of approximately 0.998. The amplifier provides a low impedance analog output (less than 1000 ohms) to drive the telemetry circuits.

To bracket the expected experimental conditions, the electrometer was required to operate over a current range of approximately 10,000 to 1. A scale compression of 10 to 1 was decided upon as a practical figure giving a 5000 to 1 range.

A 653C4 diode is used as a nonlinear element in a positive feedback loop to get the desired 10 to 1 scale compression. The input resistor is returned to a divider giving a 0.9 positive feedback resulting in an effective input resistance of 10 times the actual resistance (2×10^{10} ohm). As input current is applied the output voltage increases, and this increased voltage applied across the diode results in a reduction of the diode resistance and a consequent reduction of the positive feedback. When the output exceeds approximately 0.5 volt, the resistance of the diode is low enough to reduce the positive feedback to zero and the input resistance to 2×10^{10} ohms. A thermistor is used to compensate for the effect of temperature on the diode. For greater scale compression the use of a diode is possible in series with the input resistor, but temperature effects are serious at such extremely high resistances.

The electrometer should read zero at the end of each voltage sweep (zero volts on the plates), since no protons can then reach the collector. The zero current input will not necessarily result in a zero output because of amplifier drift. In order to correct the drift, the relay is actuated during the time of zero current input. When the relay is actuated, the positive feedback is shorted and a 1 μf capacitor is charged to a voltage equal to the amplifier drift. Upon release of the relay, the capacitor is inserted in the input circuit in such a manner that it cancels the error voltage introduced by input drift.

The instrument operates satisfactorily from -55° F to $+150^{\circ}$ F, and under extreme vibration conditions. The circuits are all designed to allow a wide tolerance in the value of the electronic components. Each circuit was tried with transistors of a wide range to determine the maximum usable limits of β and I_{CBO}. While unselected transistors are suitable in all cases, selected transistors were used in the actual construction to center the characteristics between the upper and lower maximum limits. All components used have been derated considerably.

SECOND INSTRUMENT

Design and Characteristics

The second unit was also designed with a specific payload in mind, the lunar orbiting Able V vehicle. Proton energies expected from the steady background and from solar winds in the vicinity of the moon vary from a few ev to 20 kev. The corresponding expected particle concentrations are 10^2 to 10^5 protons/cm^3. The resulting estimates of current, for a 1 cm^2 slit, are 10^{-8} to 10^{-6} amp for winds and 10^{-11} to 10^{-14} amp for the thermal background. In view of the difficulties expected in measuring the thermal proton distribution, it was decided to optimize the design for the kev range and make provision for getting order-of-magnitude data in the thermal range.

A 4 0 3

The telemetering bandwidth and the sampling rate allocated to the instrument made it impossible to obtain detailed information on the direction of the proton wind. The analyzer plates were therefore made spherical, and the instrument was located in the payload in such a way that the plane of large angular acceptance included the payload spin axis (see sketch (g)). Almost the entire solid angle is thus sampled in each revolution about the spin axis. The peak and the average values of the current over a revolution are recorded so that the degree of anisotropy in the proton distribution can be estimated. Restrictions imposed by the telemetry further dictated that the analyzer plate voltage be "stepped" rather than continuously swept. The instrument is designed to sample energies at 32 separate energy levels. The energy steps used are logarithmically related to preserve accuracy at the lower voltages (fig. 6).

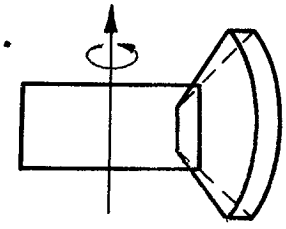

Sketch (g)

The instrument is shown in figure 7. Its spherical plates are stepped in voltage to a maximum of 3000 v, corresponding to a 19.7-kev proton energy (fig. 6). The energy acceptance, $\Delta E/E$, is approximately 0.034; the slit area is 0.40 cm^2. The sensitivity ranges are 10^{-12} to 10^{-7} amp (average current) and 10^{-11} to 4×10^{-7} amp (peak current). These ranges give a margin of safety of 4 orders of magnitude below the expected wind fluxes and thus overlap the expected thermal flux range. The weight of the instrument is 1.1 pounds, and its peak power consumption is 145 mw (110 mw av). (The power is provided by the payload solar cell and converter system.) The instrument operates properly from -55° F to +150° F and is designed to accept components with wide tolerance limits as previously described.

Electronics

The circuit diagram of the second instrument is shown in figure 8. The basic circuits are similar to those of the first instrument, but a considerable number of modifications were made to fit the requirements of a different telemetry system and vehicle mission. The first major change was the elimination of batteries, since the primary power source of the Able V payload was to be a solar cell system designed for one year of operation. The second major change was required by a narrow bandwidth digital telemetry unit. Thirdly, the electrometer circuit was changed to accommodate the new trajectory.

The vehicle provided +16 v ±1 percent; +6 v ±1 percent; and -6 v ±1 percent, from the solar cell and battery power system for operation of the instrument. The +16 v and +6 v provide suitable voltages for the high-voltage sweep circuit without major circuit changes except for a 4200-turn secondary winding in the transformer to provide the ±1500 v required. The floating battery voltages used in the electrometer were replaced by an inverter-rectifier system driven by an 8 kc square wave. A signal from this oscillator is used in the high-voltage sweep circuit to replace the 8-kc multivibrator previously required. The inverter is essentially a conventional one except that an RC timing circuit is used to maintain a stable frequency for the operation of the high-voltage transformer. The RC circuit is coupled into the feedback circuit so as to maintain near-perfect symmetry under all operating conditions. A good symmetrical waveform reduces the filtering necessary after rectification.

The feedback voltage-regulation system and the pulse technique to reduce core losses are the same as previously described. The circuit details are slightly changed, but the feedback principle of operation is the same. Most of the 2N338 transistors have been changed to 2N718 silicon mesa transistors because of a smaller size (TO-18 case). The 2N718 with its high current rating replaced the 2N549. The sweep circuit waveform is changed from a linear saw-tooth to a staircase. A trigger pulse obtained from the telemetering after each reading steps the H.V. to a new level. There are 32 voltage steps after which the cycle is repeated. A group of diodes and summing resistors are connected to the binaries to give a nonlinear sweep voltage. Since the analyzer has a constant energy resolution, it is desirable to sweep the voltage in constant percentage steps, which results in a nonlinear curve as shown in figure 6. A signal is fed to the electrometer circuit from the last binary step for sweep identification.

The electrometer tube and the transistor amplifier circuit are essentially the same as in the first instrument. The batteries are replaced by an inverter-rectifier system. The one major change is the use of a second tube as a nonlinear element. The use of positive feedback in the first unit increases the circuit drift while the use of a

nonlinear element (No. 5800 tube) does not. This is important because a relay correction circuit for drift is not practical with a digital telemetry unit (DTU), since the period between reset times can be many minutes as opposed to the 10-second sweep time used in the first instrument (the size of a charge-holding capacitor would be impracticably large). The improved stability obtained by elimination of the positive feedback, the greater voltage output to the telemetry system, and the reduced accuracy of the telemetry system (2 percent) made it practical to eliminate the relay. The No. 5800 tube used in the input acts as a diode with a calibration curve as shown in figure 9.

The electrometer has a very good frequency response considering its sensitivity. This characteristic is achieved through the use of a driven shield (around the collector) that neutralizes most of the input capacity. The response to a transient gives an RC time constant of 0.02 sec at 10^{-12} amp. At greater current levels the response is considerably better since the input resistance is lower and consequently the RC time constant is smaller. Inadequate frequency response of the telemetering system, however, made it impossible to obtain the desired angular resolution, so that it was decided to make use of two data channels and take an average reading and a peak reading in order to detect directional effects. The peak reading is read on a lower accuracy data channel (6 percent). A sweep identification signal is applied to the peak reading channel as follows: When the voltage on the plates is zero, a bias is applied to the peak reading while the average reads zero. A zero-drift in the amplifier reads on the average channel and can be used to correct the readings since the collection current will be zero when the plates are at zero voltage.

CALIBRATION AND METHOD OF DATA REDUCTION

The problems encountered in the calibration and data-reduction procedures for the two units were quite similar. These precedures will be described here for the second unit (spherical geometry).

Two of the needed sets of calibration curves were obtained in very straightforward fashion. First, the voltage output of the electrometer circuit was measured as a function of current to the collector (fig. 9). This current was supplied from a known current source. Second, the analyzer plate voltage was measured as a function of the step-number of the sweep (the plate voltage is changed in 32 steps on signal from the DTU; see fig. 6). These calibrations were performed in the payload with all flight instruments installed so that they are corrected for electrical interactions. Their dependence on payload temperature was recorded. The temperature variations were generally less than 5 percent within the maximum expected operating range, from 5° C to 35° C, and less than 10 percent from -45° C to +65° C.

The most difficult part of the calibration was the determination of the acceptance function $f(y, \theta, \varphi, \epsilon)$ of equation (13). It is not possible to determine f accurately theoretically because of unknown edge effects and secondary electron emission characteristics. Since f plays a crucial role in the interpretation of the electrometer output in terms of particle densities and angles of incidence, the experimental method of determining it and its use in reducing the data will now be described in some detail.

The instrument to be calibrated was mounted in a specially designed vacuum chamber in which it could be translated and rotated without breaking the vacuum. The chamber was installed in place of the target chamber of the Ames 8-kv ion accelerator. This apparatus, which has been more fully described by Bader, Witteborn, and Snouse (ref. 17), can deliver mass-separated beams of protons in the 20-ev to 8-kev range with an energy dispersion half-width of about 20 ev. The available proton currents, up to 200 μa, were more than adequate for calibration purposes.

A 4 0 3

The quantity to be determined experimentally was the ratio of collector current to current entering the slit, I_c/I_e, as a function of proton beam energy and the polar and azimuthal angles of incidence at a series of fixed analyzer plate voltages. For fixed azimuthal and polar angles of incidence, I_c/I_e was first measured at a fixed beam energy as a function of plate voltage. This procedure was followed because a variation of beam energy cannot be made in the accelerator without an attending variation of I_e as a result of the dependence of focusing on energy. The measurements were then repeated at a series of combinations of azimuthal and polar angle settings obtained through rotations of the instrument with respect to the beam. Finally, the entire procedure was repeated at a large number of beam energies. The desired curves of I_c/I_e at any fixed plate voltage are obtained by cross-plotting these data.

Some difficulty was encountered in measuring I_e, the current through the instrument's entrance slit. The best technique found so far was to measure the plate current in the absence of plate voltage. Under these conditions, it could be presumed that nearly all of the entering protons hit the plates, and that most of the secondary electrons produced were simply exchanged between the plates and did not contribute to the total current. There remained, however, a possible error estimated at less than ±20 percent because of secondary electron exchange between the entrance slit and the plates. Note that this introduces an uncertainty in the beam density, but not in its energy. As improved techniques for measuring I_e are devised, a correction factor to the present calibration can be introduced.

No mention has so far been made of the dependence of f on y and z, the entrance point of the beam (see sketch (d)). This dependence was experimentally eliminated by making the beam cross section larger than the slit, thus at the same time duplicating more closely the conditions to be encountered in flight. The integration of equation (13) over y yields

$$d\Phi_2 = S\left(\frac{2\epsilon_N}{m}\right)^{1/2} n(\epsilon, \theta, \varphi) f(\theta, \varphi, \epsilon, V_a) \epsilon^{1/2} \sin^2\theta \cos\varphi \, d\theta \, d\varphi \, d\epsilon \tag{20}$$

where S is the area of the slit and V_a is the analyzer plate voltage difference.

The function $n(\epsilon, \theta, \varphi)$, for the case of a monoenergetic, collimated beam from the accelerator, can be expressed in terms of δ functions:

$$n(\epsilon, \theta, \varphi) = \frac{N}{\sin\theta_o} \delta(\epsilon - \epsilon_o)\delta(\theta - \theta_o)\delta(\varphi - \varphi_o) \tag{21}$$

where ϵ_o, θ_o and φ_o are the values of ϵ, θ, and φ for the particular settings of the apparatus. Equation (20) can now be integrated to get the collector current $I_c = e\Phi_2$:

$$I_c = e\Phi_2 = eS\left(\frac{2\epsilon_N}{m}\right)^{1/2} N f(\theta_o, \varphi_o, \epsilon_o, V_a) \epsilon_o^{1/2} \sin\theta_o \cos\varphi_o$$

$$= I_e f(\theta_o, \varphi_o, \epsilon_o, V_a) \tag{22}$$

where the last form of the equation follows from the fact that $I_e = eSNu_o \sin\theta_o \cos\varphi_o$ and $u_o = (2\epsilon_N\epsilon_o/m)^{1/2}$. The relationship $f = I_c/I_e$ is, of course, the expected one for a monoenergetic, collimated beam.

Since I_c/I_e was measured for large numbers of values of θ_o, φ_o, ϵ_o, and V_a, it was then possible to plot the general function $f(\theta, \varphi, \epsilon, V_a)$ versus each of the variables. The following analytical expression was then fitted to the experimental curves:

$$f(\theta, \varphi, \epsilon, V_a) = \frac{A_1 e^{-A_2|\varphi|} + B_1 \cos B_2\varphi}{\cos\varphi} e^{\left(\frac{\epsilon - \epsilon_m}{\sigma}\right)^2} \cos\eta\left(\theta - \frac{\pi}{2}\right) \tag{23}$$

where A_1, A_2, B_1, B_2, η, ϵ_m, and σ were determined for optimum fit; the expression is valid for $85^\circ \leq \theta \leq 95^\circ$ ($\eta = 18$), $-85^\circ \leq \varphi \leq +85^\circ$, and $f = 0$ whenever either θ or φ is outside these limits. Representative plots of the experimentally determined acceptance function are shown in figures 10(a), (b), (c), and (d).

The quantities ϵ_m and σ are of some interest, since for normal incidence of the beam on the slit they are related to the analyzer constant E_a/eV_a of equation (3) and the energy acceptance $\Delta E/E_a$ of equation (10). It was found experimentally that $\sigma = 0.034\ \epsilon_m$ and $\epsilon_m = 6.8\ eV_a/\epsilon_N$. From equations (3) and (10) and the known plate radii, one would predict $\sigma \approx 1/2\ \Delta E/\epsilon_N = 0.040\ \epsilon_m$ and $\epsilon_m = E_a/\epsilon_N = 6.3\ eV_a/\epsilon_N$. The agreement is satisfactory in view of departures from plate sphericity affecting Δr and of the large edge effects to be expected, since the entrance and exit slits of the analyzer were made as wide as the plate separation in order to accept the largest possible current.

Equation (23) does not take into account a slight observed dependence of the θ term on the value of ϵ. The resulting uncertainty in θ is $\pm 6^\circ$.

A
4
0
3

There remains, then, only to discuss how $n(\epsilon, \theta, \varphi)$ can be deduced from the telemetered information. If the proton velocity distribution is isotropic, then of course

$$I_{c_{av}} = I_{c_{max}} \tag{24a}$$

If the velocity distribution is unidirectional,

$$I_{c_{av}} = \frac{I_{c_{max}}}{2\pi} \int_{\frac{\pi}{2} - \frac{\pi}{2\eta}}^{\frac{\pi}{2} + \frac{\pi}{2\eta}} \cos \eta \left(\theta_o - \frac{\pi}{2}\right) \sin \theta_o d\theta_o = 0.018\ I_{c_{max}} \tag{24b}$$

where the numerical constant was evaluated for $\eta = 18$. If the θ dependence of the velocity distribution is peaked about θ_o, in the form

$$e^{-\frac{(\theta - \theta_o)^2}{\nu^2}}$$

then

$$I_{c_{av}} = \frac{\frac{1}{\pi}\int_{-\frac{\pi}{2}}^{\frac{\pi}{2}} d\theta_o \int_{\frac{\pi}{2}-\frac{\pi}{2\eta}}^{\frac{\pi}{2}+\frac{\pi}{2\eta}} e^{-\left(\frac{\theta-\theta_o}{\nu}\right)^2} \cos\eta\left(\theta-\frac{\pi}{2}\right)\sin\theta\, d\theta}{\int_{\frac{\pi}{2}-\frac{\pi}{2\eta}}^{\frac{\pi}{2}+\frac{\pi}{2\eta}} e^{-\left[\frac{\theta-(\pi/2)}{\nu}\right]^2} \cos\eta\left(\theta-\frac{\pi}{2}\right)\sin\theta\, d\theta} I_{c_{max}}$$

$$\approx \frac{\nu}{2\sqrt{\pi}} \frac{\operatorname{erf}\frac{\pi}{\nu}}{1 - \frac{\left(\frac{\pi}{2}\right)^2 - 2}{(\eta\nu)^2} + \frac{\left(\frac{\pi}{2}\right)^4 - 12\left(\frac{\pi}{2}\right)^2 + 24}{2(\eta\nu)^4}} I_{c_{max}}$$

$$= \begin{cases} 0.029\ I_{c_{max}} & \nu = \frac{\pi}{36}\ (5^\circ) \\ 0.10\ I_{c_{max}} & \nu = \frac{\pi}{9}\ (20^\circ) \\ 0.42\ I_{c_{max}} & \nu = \frac{\pi}{2}\ (90^\circ) \end{cases} \qquad (24c)$$

where the approximate form is valid for θ close to $\pi/2$. This is the case for $\eta = 18$, which value was used in the numerical evaluation. It has been assumed in equations (24) that the electrometer response time is such that the value $I_{c_{max}}$ is actually registered. The actual response time of the system is such that under the most severe condition (δ-function input, eq. (24b)) about 0.95 $I_{c_{max}}$ is obtained. It is thus possible to obtain a very good approximation to the θ dependence of the proton distribution n.

The φ dependence of n is more difficult to obtain, since it is necessary that the data be compared for many values of φ. The spin of the vehicle only changes θ, so that the data at a given location have to be compared with those taken at the same place but with a different spin-axis orientation. This necessarily entails a time difference between the comparison points, and hence it can be valid only in a steady-state environment. This point will be further discussed below.

The dependence of n on energy can be obtained readily because of the high resolution of the instrument. Since $\Delta E/E_a \approx 0.05$, n and $\epsilon^{1/2}$ can be assumed constant in the integration of equation (20) over energy. Aside from constant factors (and angular dependence), the integration yields

$$I_c \propto n(\epsilon)\epsilon^{1/2}\sigma \propto n(\epsilon)V_a^{3/2} \qquad (25)$$

So far only the functional dependence of the proton distribution has been discussed. In order to obtain the number of protons per unit volume, N, it is necessary to complete the integration of equation (20). This, in turn, requires that some assumptions be made regarding the φ dependence of n. Some information should be gained from examination of the θ dependence: if, for example, n is isotropic in θ, it is probably isotropic in φ; and if n is highly peaked in θ, it is probably anisotropic in φ. Further information should be gained from data taken at different times at nearly the same location and with a different spin-axis orientation. If, as is probable, there should be a small amount of tumbling motion of the vehicle, it is possible that on consequent orbits the angles θ and φ should be interchanged. In this case, of course, the information on the φ dependence will be as good as that for the θ dependence. It should be possible to minimize the errors due to time differences by taking into account levels of particle activity generally known from other sources (such as the higher-energy particle counts of other instruments in the same payload).

The task of data reduction will, in any case, be complicated and time-consuming. It is clear from the above discussion that it cannot be handled entirely by electronic computers. Some qualitative interpretations must be made on which to base the choices of trial distribution functions for use in the integrations, and judgment must be passed on the adequacy of the results. Electronic computers will, however, handle the otherwise overwhelming job of translating the raw telemetered data into collector currents, correlated with plate voltages and with orbital spatial and temporal parameters too numerous to list at this point. It is hoped that the careful examination of the data obtained during the first few weeks in orbit will lead progressively to their almost complete handling by computers.

Ames Research Center
National Aeronautics and Space Administration
Moffett Field, Calif., April 25, 1961

REFERENCES

1. Hoyle, F., and Lyttleton, R. A.: The Effect of Interstellar Matter on Climatic Variation. Proc. Cambridge Phil. Soc., vol. 35, 1939, pp. 405-592.

2. Friedman, Herbert: IGY Solar Flare Program and Ionizing Radiation in the Night Sky. Amer. Rocket Soc. Jour., vol. 29, no. 2, Feb. 1959, pp. 103-107.

3. Lilley, A. E.: Association of Gas and Dust from 21-cm Hydrogen Radio Observations. Astrophysical Jour., vol. 121, no. 3, May 1955, pp. 559-568.

4. Storey, O.: Protons Outside the Earth's Atmosphere. Annales de Geophysique, vol. 14, 1958, p. 144.

5. Johnson, Francis S.: The Structure of the Outer Atmosphere Including the Ion Distribution Above the F-2 Maximum. Lockheed Tech. Rep. LMSD-49719, April 28, 1959.

6. Chapman, S.: Notes on the Solar Corona and the Terrestial Ionosphere. Smithsonian Contributions to Astrophysics, vol. 2, no. 1, 1957, pp. 1-11.

7. Biermann, L.: The Tail of Halley's Comet in 1910. (Über den schweif des kometen Halley im jahre 1910.) Zeitschrift für Naturforschung, v. 7A, Jan. 1952, pp. 127-136.

8. Osterbrock, Donald E.: A Study of Two Comet Tails. Astrophysical Jour., vol. 128, 1958, pp. 95-105.

9. Dodson, Helen W., and Hedeman, E. Ruth: Geomagnetic Disturbances Associated with Solar Flares with Major Premaximum Bursts at Radio Frequencies $\leq$ 200 MC/S. Jour. Geophysical Res., vol. 63, no. 1, March 1958, pp. 77-96.

10. Parker, E. N.: Interaction of the Solar Wind with the Geomagnetic Field. Physics of Fluids, vol. 1, no. 3, June 1958, pp. 171-187.

11. Parker, E. N.: Origin and Dynamics of Cosmic Rays. Physical Review, vol. 109, no. 4, Feb. 15, 1958, pp. 1328-1344.

12. Parker, E. N.: Cosmic-Ray Modulation by Solar Wind. Physical Review, vol. 110, no. 6, June 15, 1958, pp. 1445-1449.

13. Dessler, A. J.; Penetrating Radiation. Satellite Environment Handbook, LMSD-895006, Dec. 1960, pp. 3-1 to 3-35.

14. Jastrow, R., and Pearse, C. A.: Atmospheric Drag on the Satellite. Jour. Geophysical Res., vol. 62, no. 3, Sept. 1957, pp. 413-423.

15. Gringauz, K. N., and Zelikman, M. Kh.: Measurement of the Concentrations of Positive Ions Along the Orbit of an Artificial Satellite. The Russian Literature of Satellites, Part II, International Physical Index, Inc., New York, 1958, pp. 133-147.

16. Stormer, Carl: The Polar Aurora. Oxford, The Claredon Press, 1955.

17. Bader, Michel, Witteborn, Fred C., and Snouse, Thomas B.: Sputtering of Metals by Mass-Analyzed N_2^+ and N^+. NASA TR R-105, 1961.

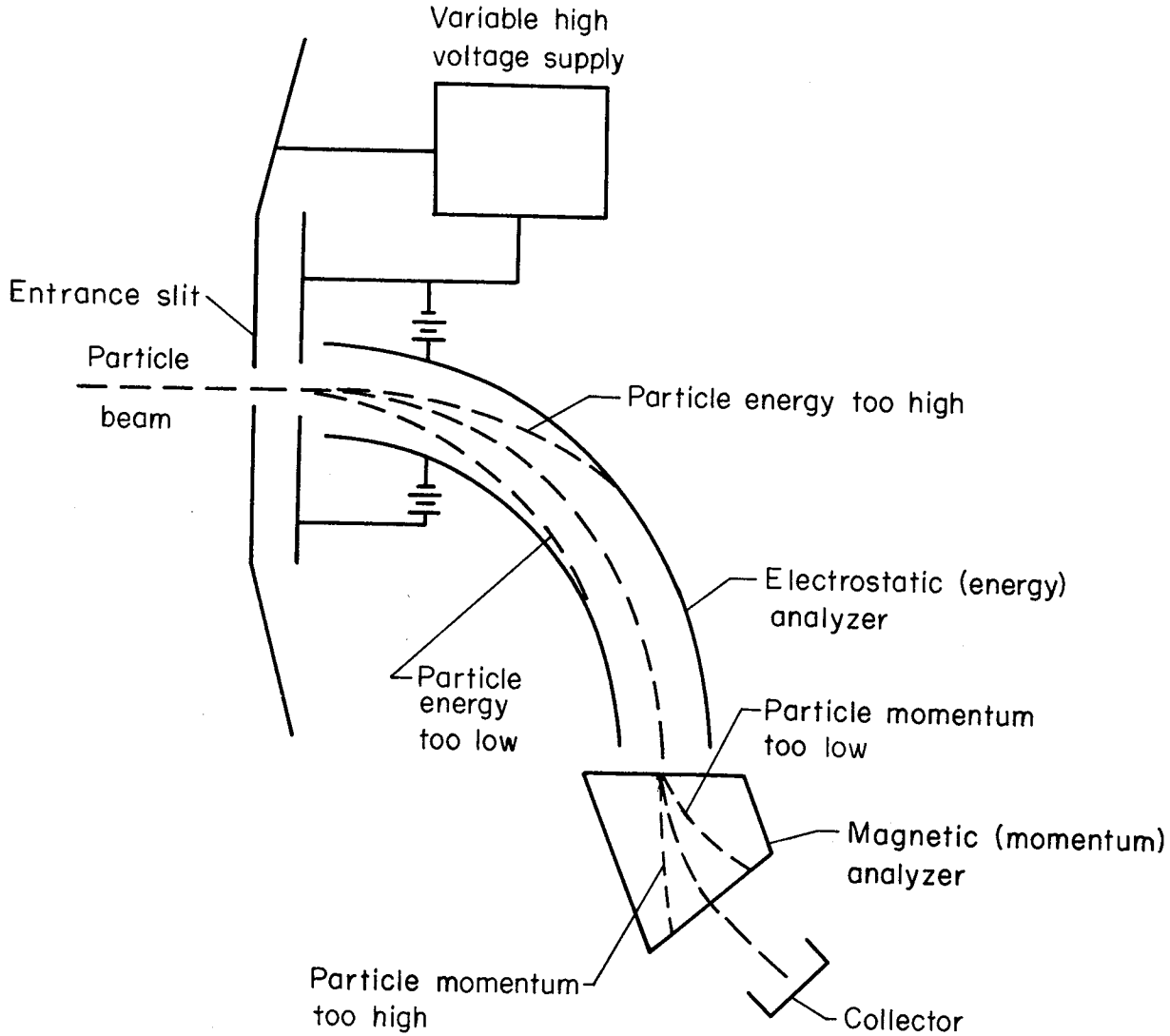

Figure 1.- Schematic drawing of an electromagnetic analyzer design suitable for space-vehicle payload application.

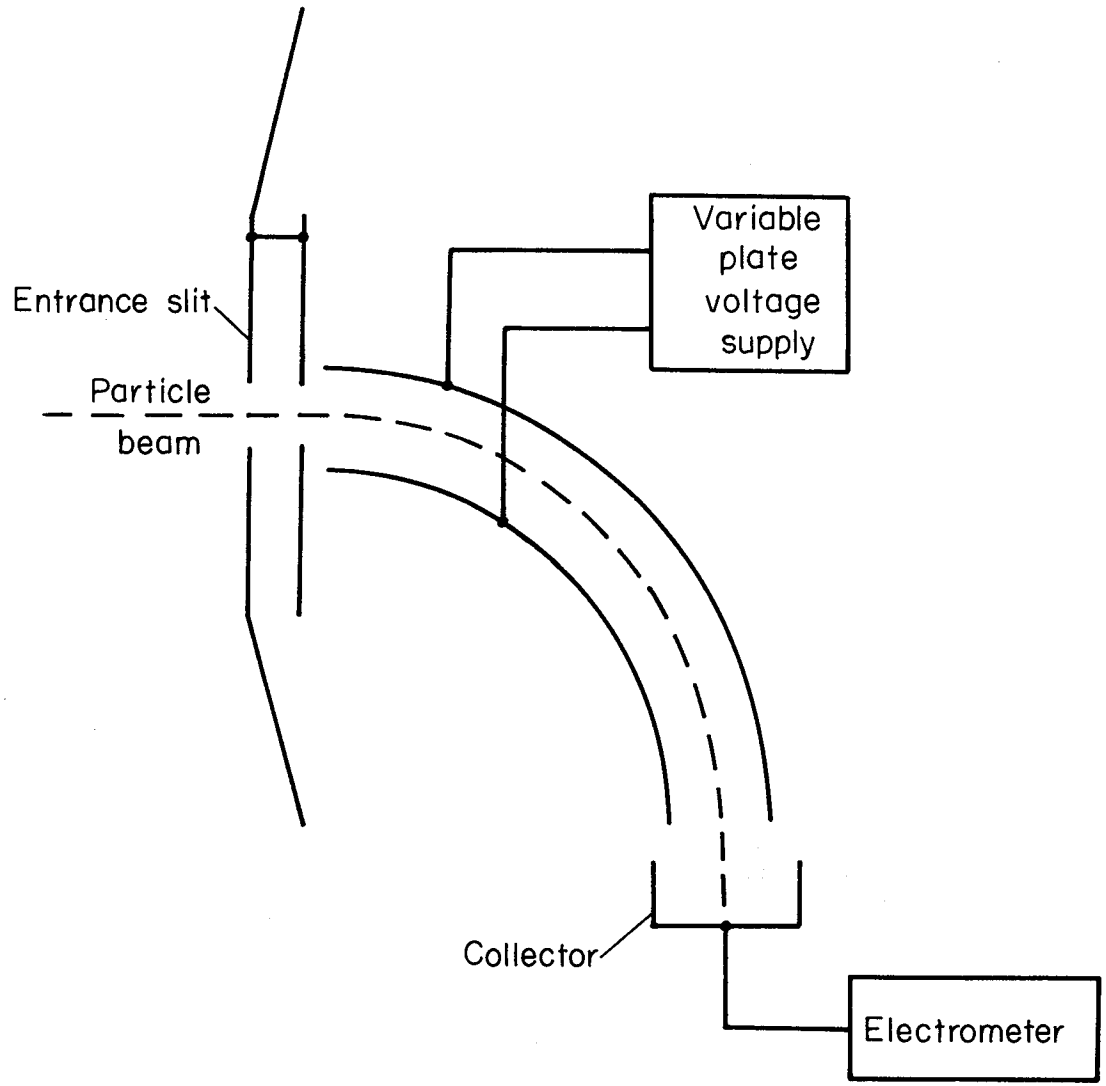

Figure 2.- Schematic drawing of electrostatic analyzer.

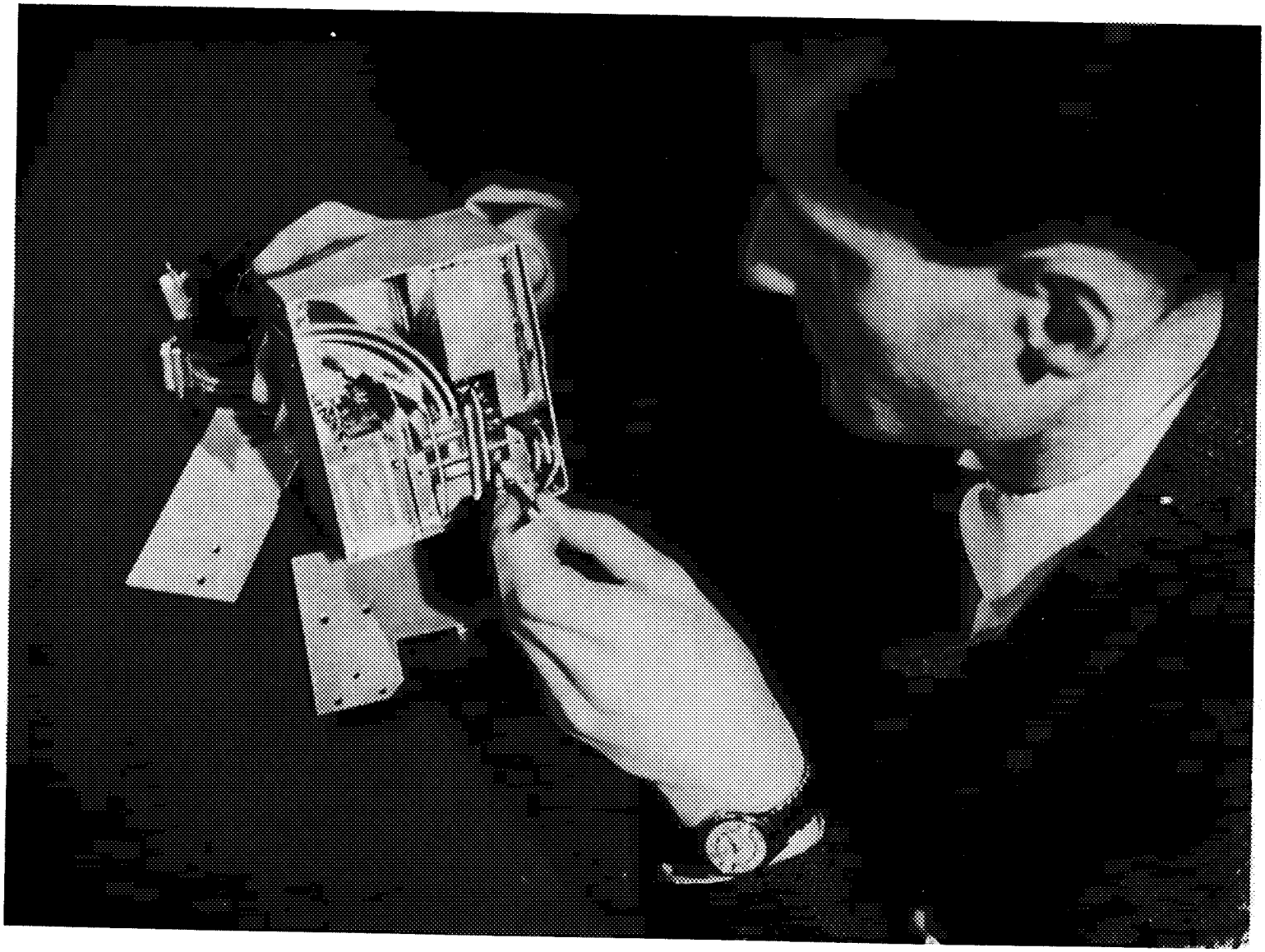

Figure 3.- First instrument (cylindrical electrostatic analyzer).

A-26108

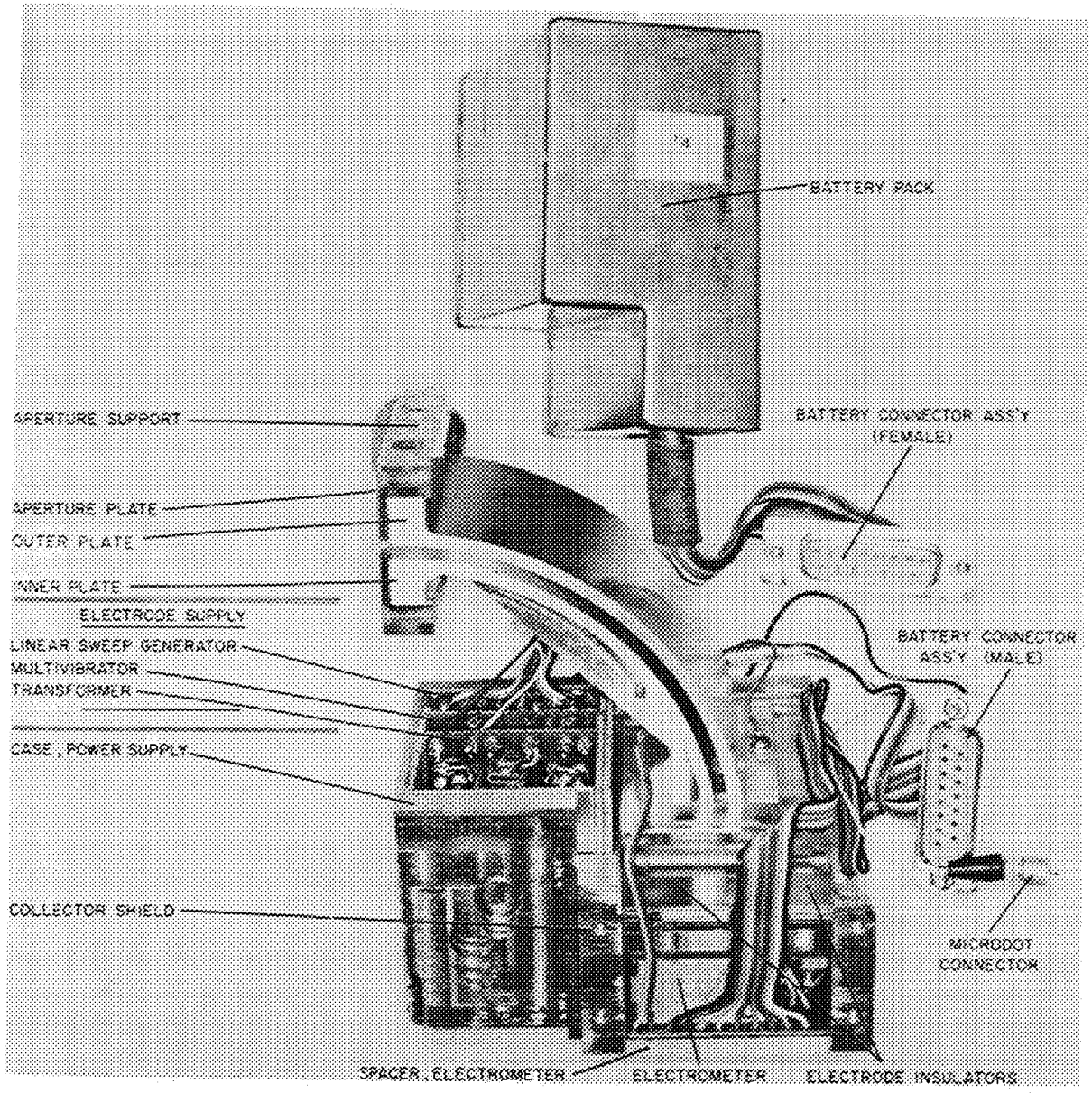

Figure 4.- Details of first instrument.

A
4
0
3

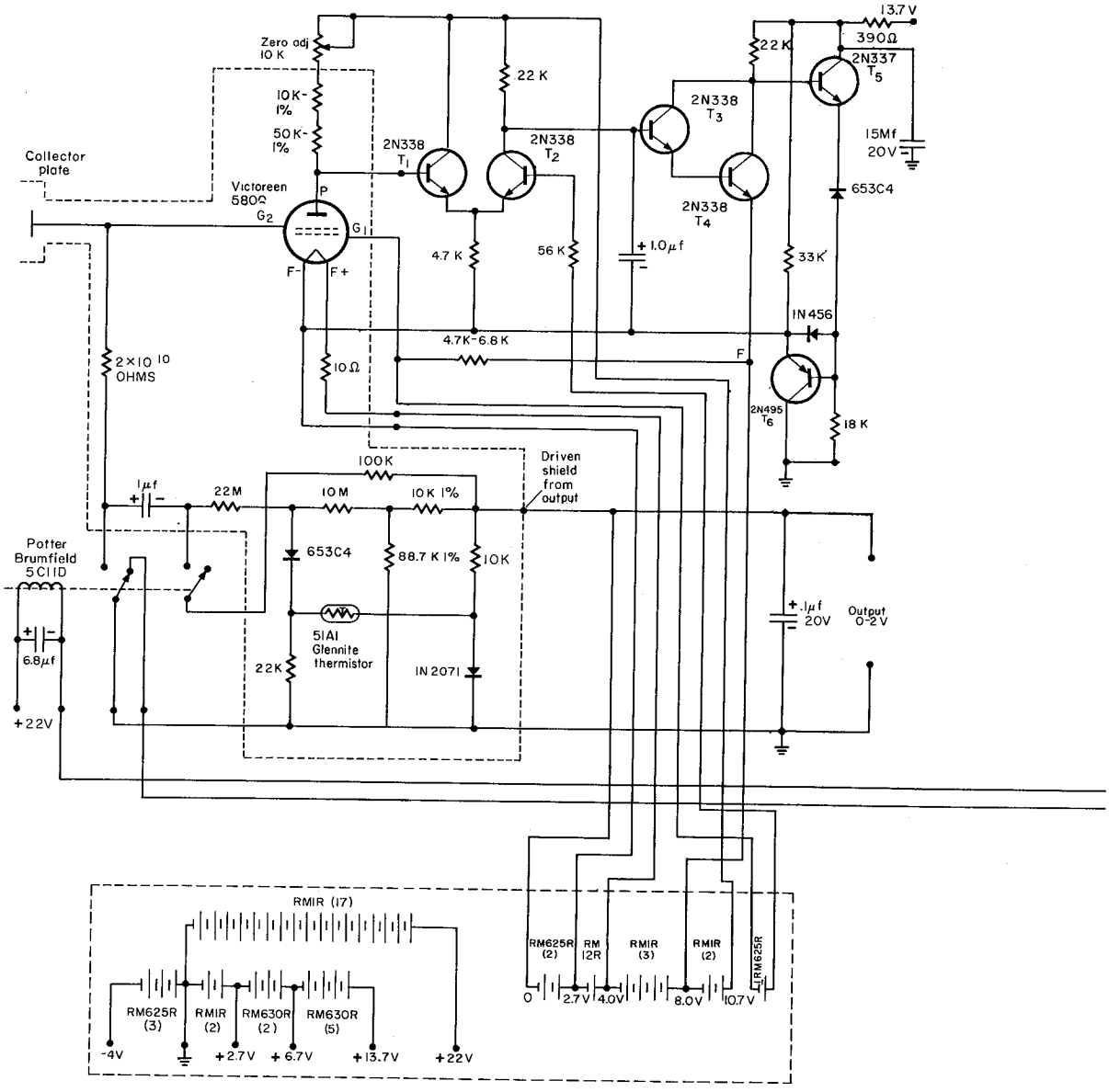

Figure 5.- Circuit diagram of first instrument.

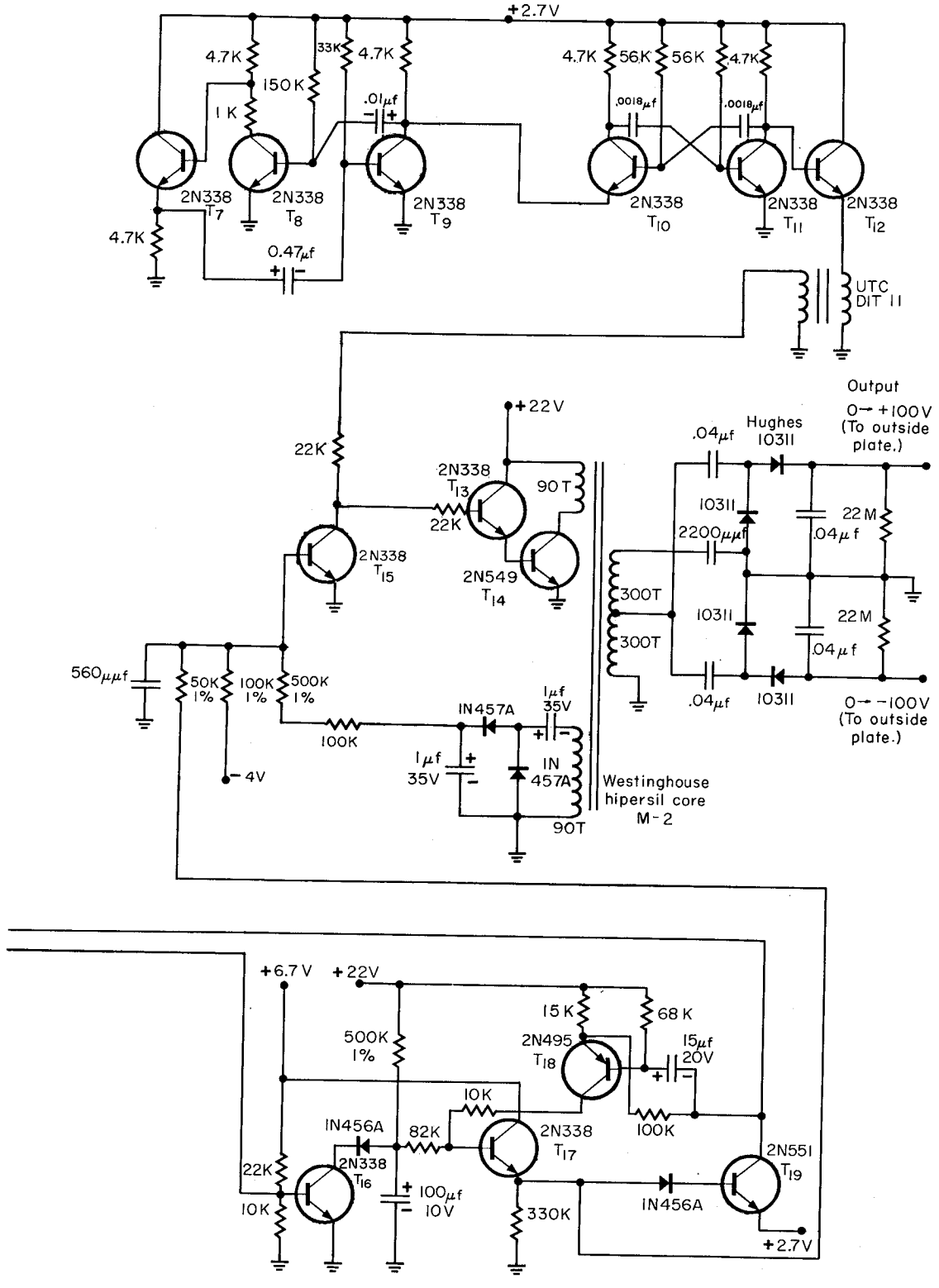

Figure 5.- Concluded.

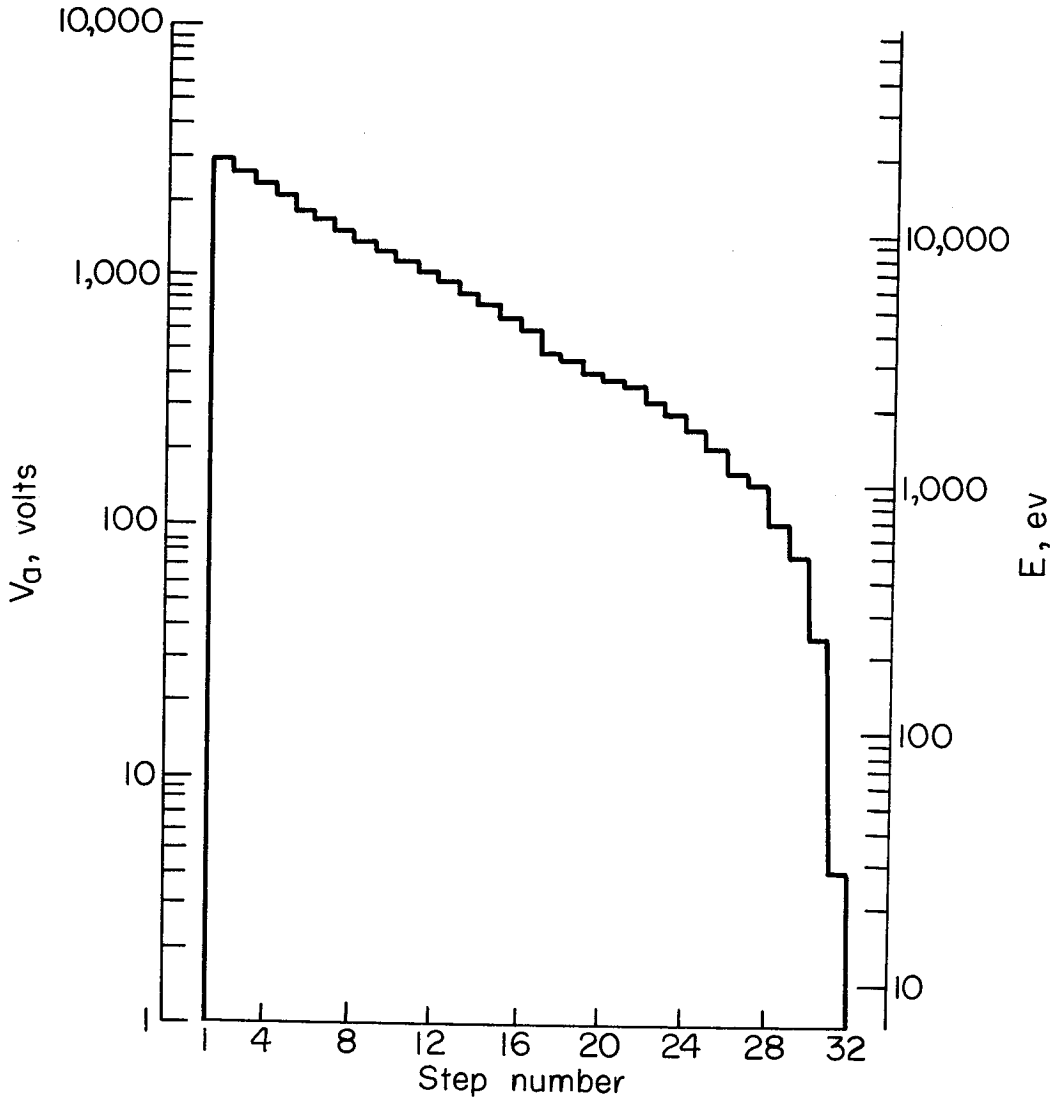

Figure 6.- Voltage across analyzer plates, V_a, and corresponding collected particle energy, E, for a 32-step cycle.

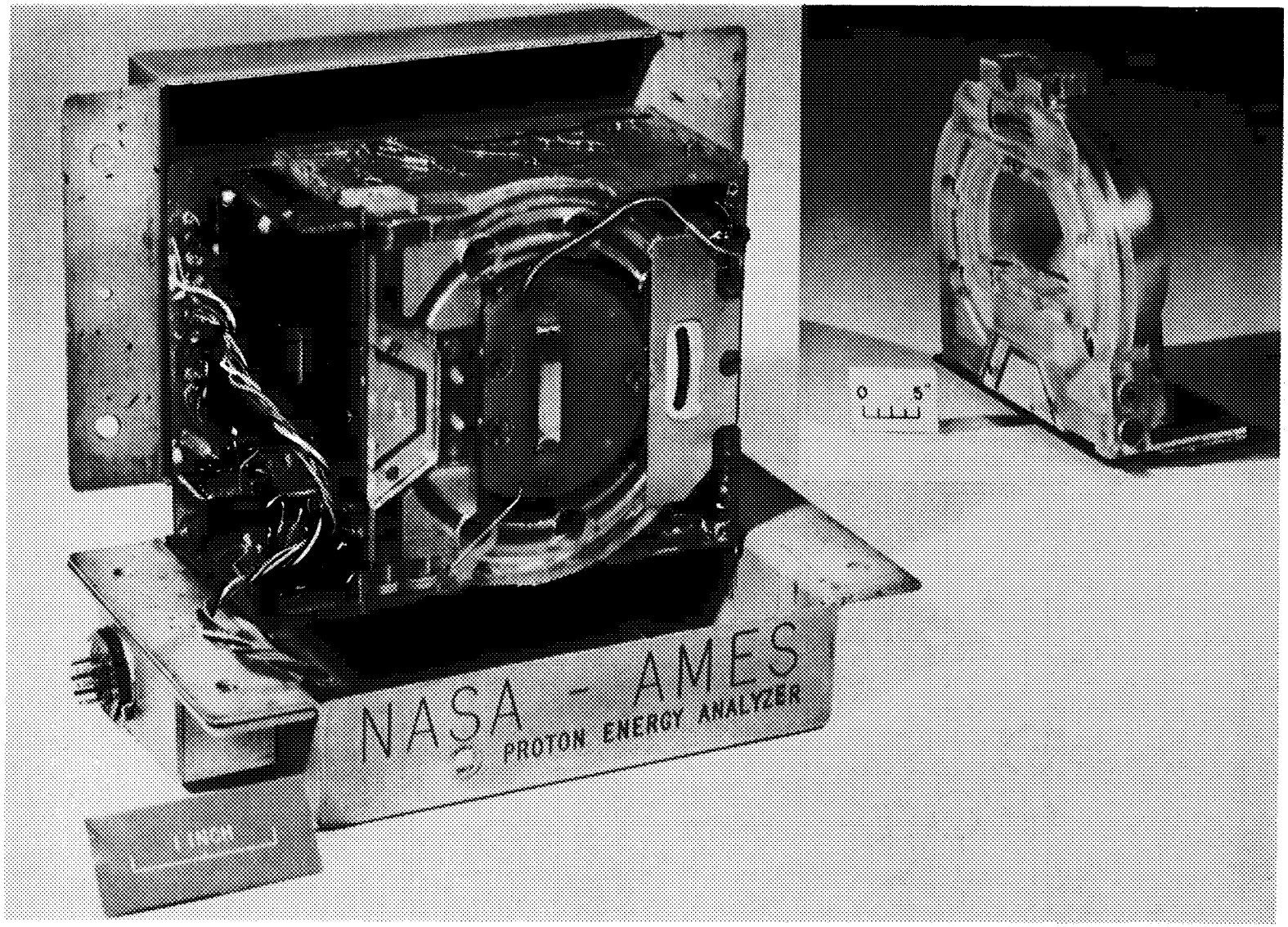

A-26969.1

Figure 7.- Second instrument (hemispherical electrostatic analyzer).

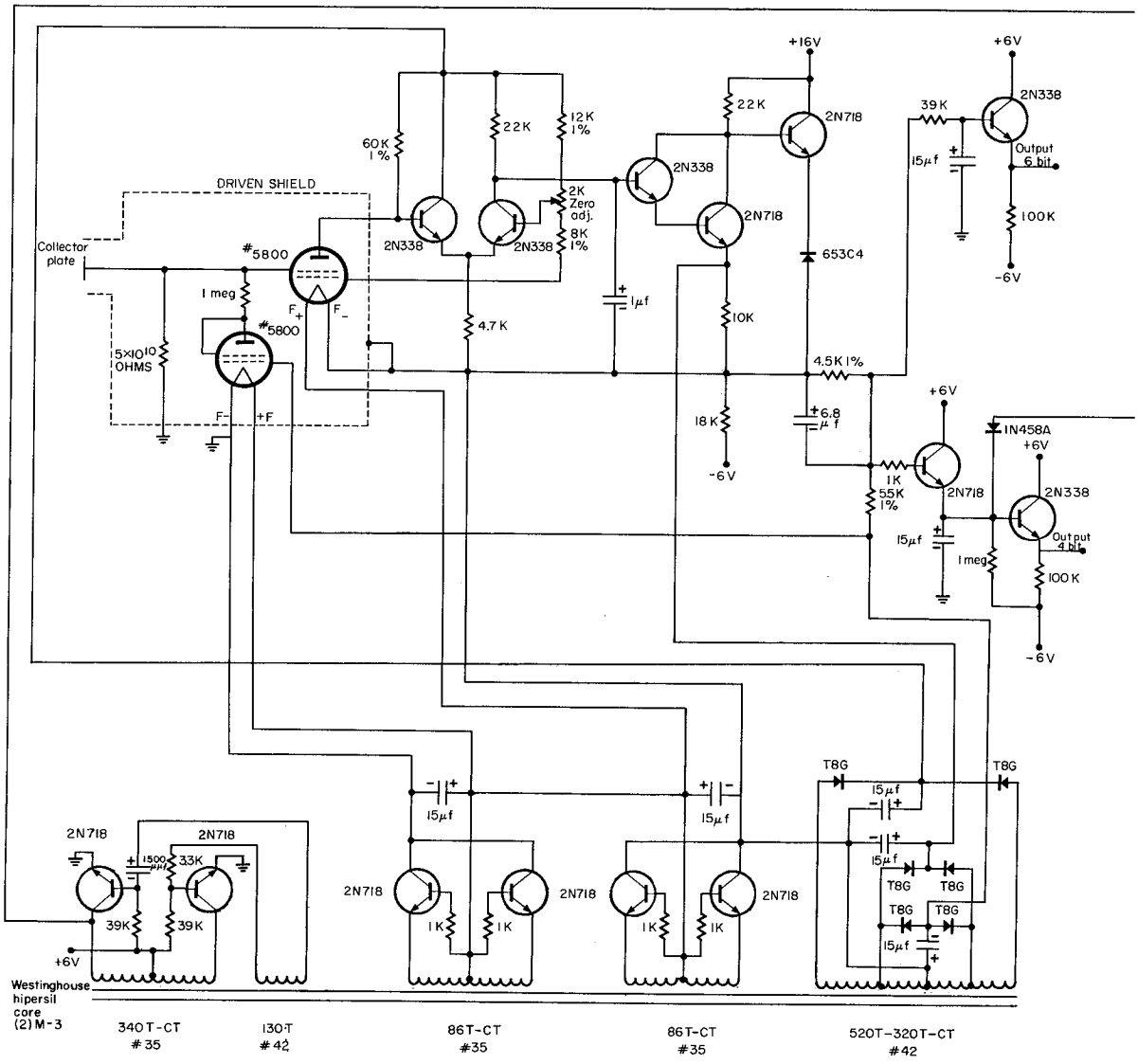

Figure 8.- Circuit diagram of second instrument.

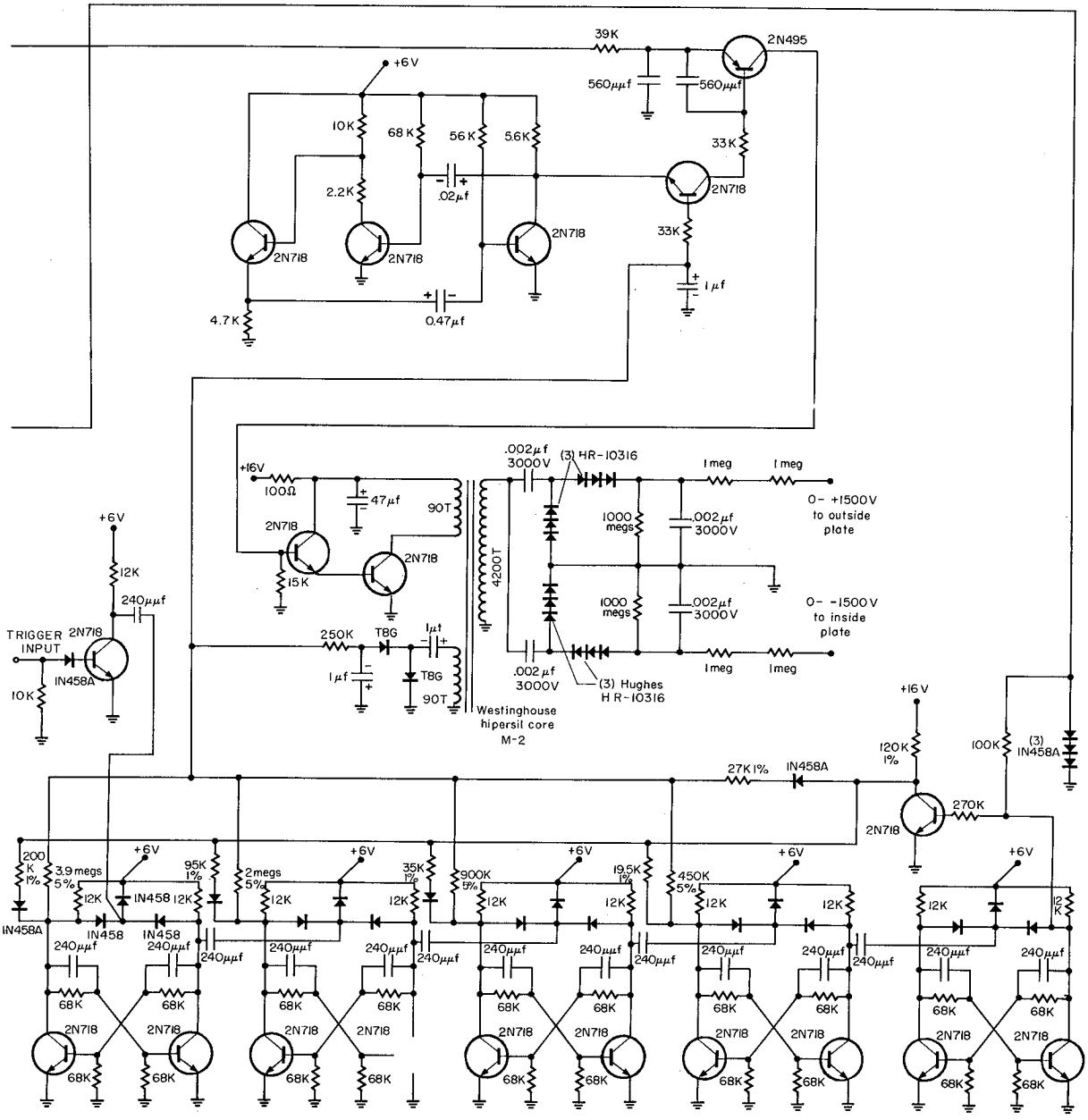

Figure 8.- Concluded.

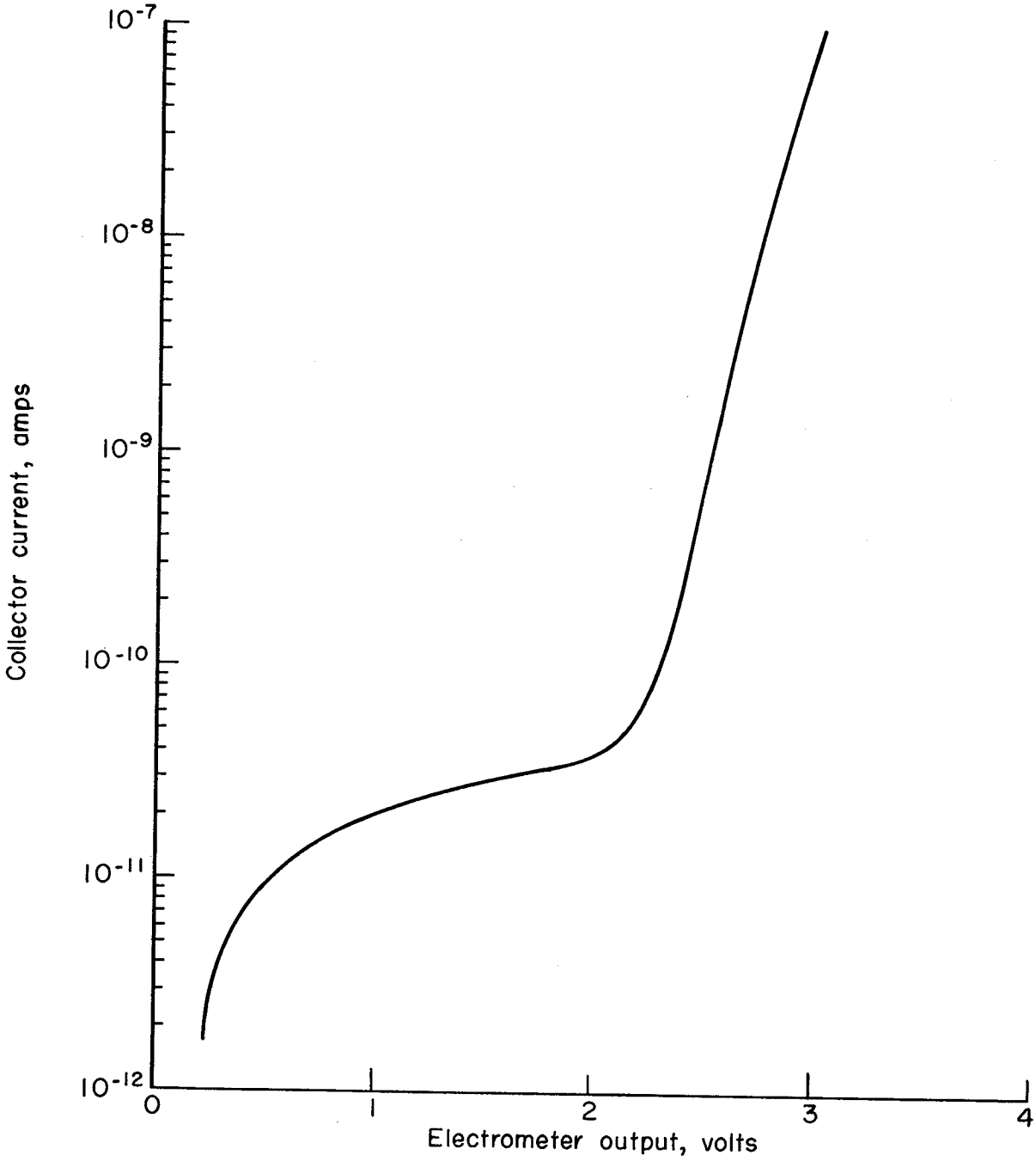

Figure 9.- Electrometer calibration curve.

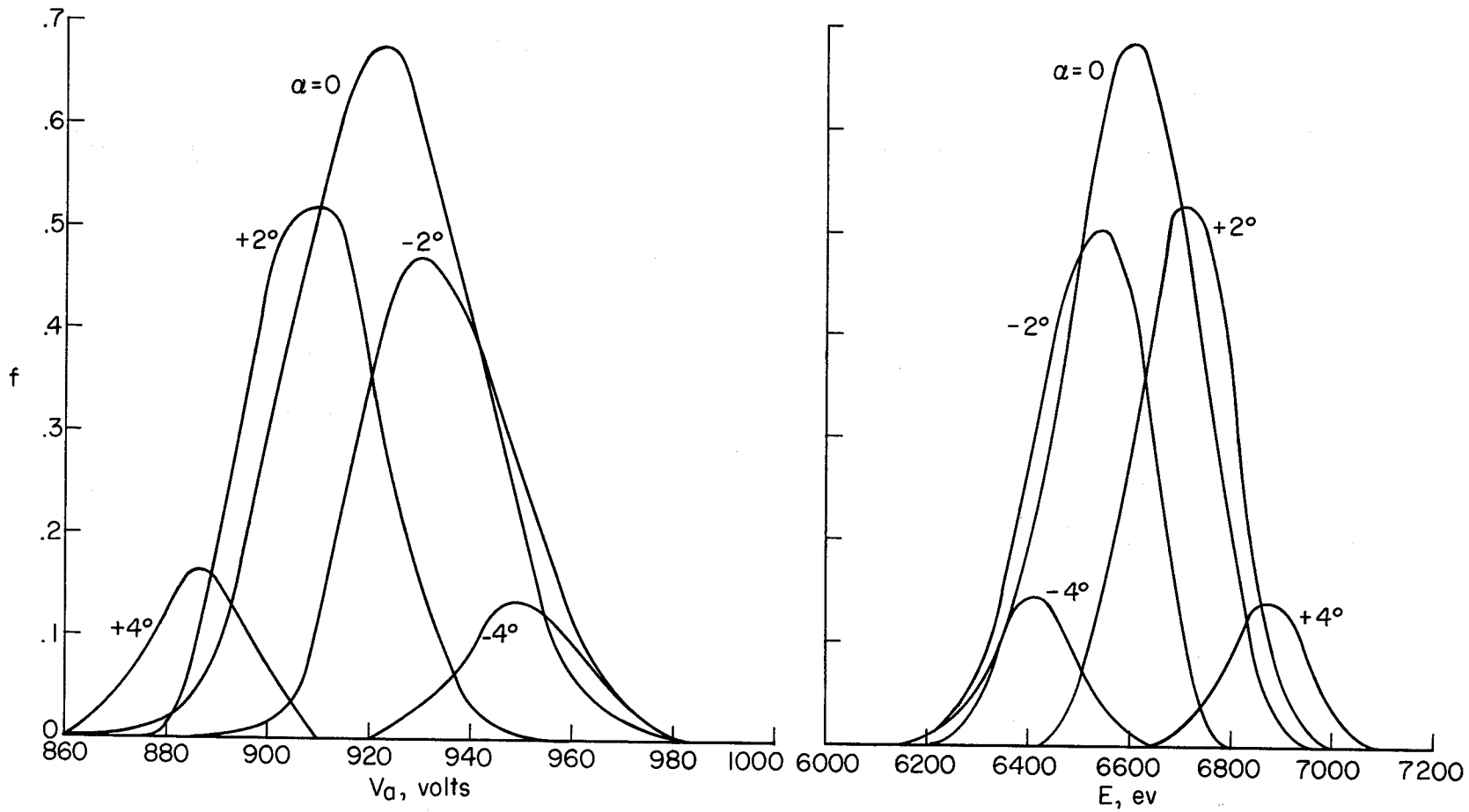

(a) f vs. V_a at $\varphi = 0$, E = 6070 ev.

(b) f vs. E at $\varphi = 0$, V_a = 1000 v.

Figure 10.- Typical calibration curves for the acceptance function f of the second instrument.

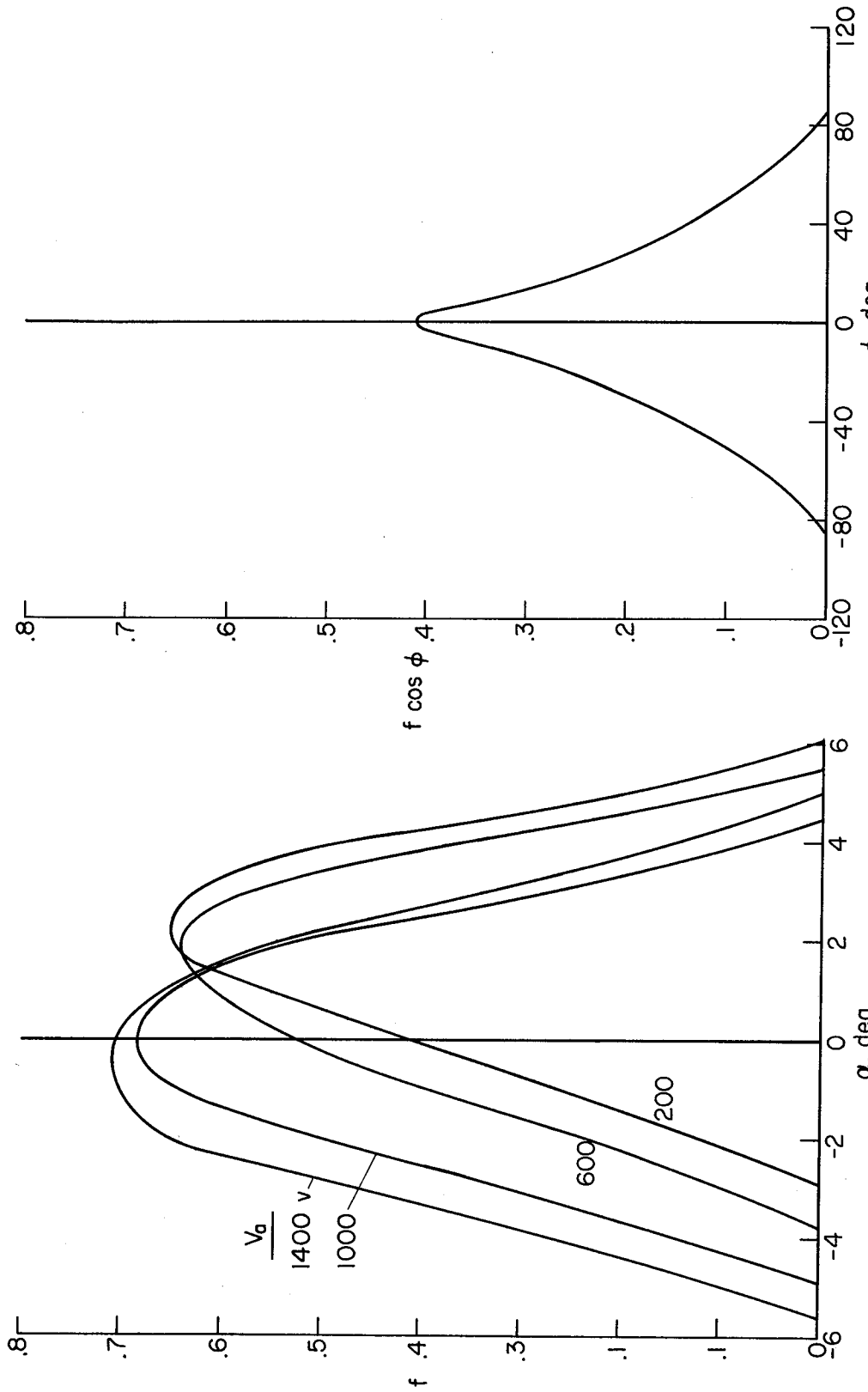

(c) f vs. α at φ = 0, ϵ = ϵ_{max}.

(d) f cos φ vs. φ at α = 0, E = 600 ev., V_a = 96 v.

Figure 10.- Concluded.

NASA TN D-1035
National Aeronautics and Space Administration.
TWO INSTRUMENTS FOR MEASURING DISTRIBUTIONS OF LOW-ENERGY CHARGED PARTICLES IN SPACE. Michel Bader, Thomas B. Fryer, and Fred C. Witteborn. July 1961. 42p. OTS price, $1.25. (NASA TECHNICAL NOTE D-1035)

Some methods and instrumentation for measuring the energy and density distribution of low-energy (0 to 20 kev) ions in space are considered from the standpoint of suitability for space vehicle payloads. It is concluded that electrostatic analysis of the energy distribution can provide sufficient information in initial experiments. Instruments designed and constructed at the Ames Research Center for space plasma measurements, and the methods of calibration and data reduction are described.

Copies obtainable from NASA, Washington

I. Bader, Michel
II. Fryer, Thomas B.
III. Witteborn, Fred C.
IV. NASA TN D-1035

(Initial NASA distribution: 6, Astronomy; 16, Cosmochemistry; 17, Communications and sensing equipment, flight; 20, Fluid mechanics; 31, Physics, nuclear and particle.)

NASA

NASA TN D-1035
National Aeronautics and Space Administration.
TWO INSTRUMENTS FOR MEASURING DISTRIBUTIONS OF LOW-ENERGY CHARGED PARTICLES IN SPACE. Michel Bader, Thomas B. Fryer, and Fred C. Witteborn. July 1961. 42p. OTS price, $1.25. (NASA TECHNICAL NOTE D-1035)

Some methods and instrumentation for measuring the energy and density distribution of low-energy (0 to 20 kev) ions in space are considered from the standpoint of suitability for space vehicle payloads. It is concluded that electrostatic analysis of the energy distribution can provide sufficient information in initial experiments. Instruments designed and constructed at the Ames Research Center for space plasma measurements, and the methods of calibration and data reduction are described.

Copies obtainable from NASA, Washington

I. Bader, Michel
II. Fryer, Thomas B.
III. Witteborn, Fred C.
IV. NASA TN D-1035

(Initial NASA distribution: 6, Astronomy; 16, Cosmochemistry; 17, Communications and sensing equipment, flight; 20, Fluid mechanics; 31, Physics, nuclear and particle.)

NASA

NASA TN D-1035
National Aeronautics and Space Administration.
TWO INSTRUMENTS FOR MEASURING DISTRIBUTIONS OF LOW-ENERGY CHARGED PARTICLES IN SPACE. Michel Bader, Thomas B. Fryer, and Fred C. Witteborn. July 1961. 42p. OTS price, $1.25. (NASA TECHNICAL NOTE D-1035)

Some methods and instrumentation for measuring the energy and density distribution of low-energy (0 to 20 kev) ions in space are considered from the standpoint of suitability for space vehicle payloads. It is concluded that electrostatic analysis of the energy distribution can provide sufficient information in initial experiments. Instruments designed and constructed at the Ames Research Center for space plasma measurements, and the methods of calibration and data reduction are described.

Copies obtainable from NASA, Washington

I. Bader, Michel
II. Fryer, Thomas B.
III. Witteborn, Fred C.
IV. NASA TN D-1035

(Initial NASA distribution: 6, Astronomy; 16, Cosmochemistry; 17, Communications and sensing equipment, flight; 20, Fluid mechanics; 31, Physics, nuclear and particle.)

NASA

NASA TN D-1035
National Aeronautics and Space Administration.
TWO INSTRUMENTS FOR MEASURING DISTRIBUTIONS OF LOW-ENERGY CHARGED PARTICLES IN SPACE. Michel Bader, Thomas B. Fryer, and Fred C. Witteborn. July 1961. 42p. OTS price, $1.25. (NASA TECHNICAL NOTE D-1035)

Some methods and instrumentation for measuring the energy and density distribution of low-energy (0 to 20 kev) ions in space are considered from the standpoint of suitability for space vehicle payloads. It is concluded that electrostatic analysis of the energy distribution can provide sufficient information in initial experiments. Instruments designed and constructed at the Ames Research Center for space plasma measurements, and the methods of calibration and data reduction are described.

Copies obtainable from NASA, Washington

I. Bader, Michel
II. Fryer, Thomas B.
III. Witteborn, Fred C.
IV. NASA TN D-1035

(Initial NASA distribution: 6, Astronomy; 16, Cosmochemistry; 17, Communications and sensing equipment, flight; 20, Fluid mechanics; 31, Physics, nuclear and particle.)

NASA